Lithos 318–319 (2018) 419–433

Contents lists available at ScienceDirect

Lithos

journal homepage: www.elsevier.com/locate/lithos

Fate of fluids at the base of subcratonic lithosphere: Experimental constraints at 5.5–7.8 GPa and 1150–1350 deg C

Alexander G. Sokol [a,b,*], Anatoly A. Tomilenko [a], Taras A. Bul'bak [a], Alexey N. Kruk [a,b], Ivan A. Sokol [a], Yury N. Palyanov [a,b]

[a] V.S. Sobolev Institute of Geology and Mineralogy, Siberian Branch of the Russian Academy of Sciences, ave. Koptyuga 3, Novosibirsk, 630090, Russia
[b] Novosibirsk State University, str. Pirogova 2, Novosibirsk, 630090, Russia

ARTICLE INFO

Article history:
Received 24 February 2018
Accepted 21 August 2018
Available online 27 August 2018

Keywords:
mantle
experiment
fluid
hydrocarbons
metasomatism
deep carbon and nitrogen cycles

ABSTRACT

Phase relations in the lherzolite-C-O-H-N system are studied experimentally at 5.5–7.8 GPa, 1150–1350 deg C, and oxygen fugacity (fO_2) from 2.5 log units below to 3.5 log units above the iron-wüstite (IW) equilibrium, in 10- to 150-h runs. The two-capsule technique is applied to maintain hydrogen fugacity (fH_2) at the IW (Fe-FeO), MMO (Mo-MoO_2), and HM (Fe_2O_3-Fe_3O_4) equilibria. The mineral assemblage stable in the Fe^0- and graphite-saturated lherzolite-C-O-H-N system, at 6.3–7.8 GPa and 1200–1350 deg C, consists of olivine, orthopyroxene, clinopyroxene, and garnet. The metal phase occurs either as iron carbide (Fe_3C) or iron nitride (Fe_3N) at low and high concentrations of nitrogen, respectively. Carbide and nitride phases contain progressively more Ni (5–6 to 25 wt.%) as fluids become more hydrous. Fluids equilibrated with lherzolite consist of CH_4 and C_2H_6, minor amounts of other alkanes, H_2O, NH_3, and methaneimine (CH_3N). Fluids with high nitrogen contents are mainly composed of NH_3, N_2, light alkanes, and water. As fO_2 increases, Fe_3C and Fe_3N oxidize and silicate phases (olivine, orthopyroxene, and garnet) contain more FeO, while fluids become richer in H_2O and more depleted in hydrocarbons (HCs). Fluids synthesized at lithospheric $P = 5.5$–6.3 GPa, $T = 1150$–1200 deg C and fO_2 near the carbon-saturated water maximum (CW) contain up to 85 rel.% H_2O and at least 14 rel.% of total HCs. The presence of HCs stable to oxidation suppresses water activity in fluids while the solidus of the lherzolite-C-O-H-N system at fO_2 near CW becomes at least 150 deg C higher than that of the carbon-free lherzolite-H_2O system. Further oxidation of HCs and C^0 leads to partial carbonation of olivine and orthopyroxene and their replacement by magnesite and clinopyroxene. The total content of HCs (mainly C_2-C_{13} alkanes and oxygenated HCs) in fluids from magnesite-bearing lherzolite at 5.5 GPa and 1200 deg C is never below 9 rel.% even in 150-h runs, while CO_2 does not exceed 3–5 rel.%. Melt inclusions composed of Mg and Ca carbonates in olivine record the first batches of carbonate melt at these P-T and redox conditions. The solidus of the lherzolite-C-O-H-N system at 5.5–7.8 GPa with fO_2 between metal and carbonate saturation is above the typical upper mantle temperatures at a heat flux of 40 mW/m^2. Thus, the experiments demonstrate that HC-H_2O fluids can ascend from metal-saturated asthenosphere to more oxidized lithospheric mantle in a typical thermal regime and supply volatiles for carbonatite metasomatism and generation of carbonate-silicate melts.

1. Introduction

The upper mantle fluid regime controls the conditions of magma generation, transport of elements, and some properties of mantle rocks. The composition of mantle fluids has been universally assumed to depend mainly on oxygen fugacity (fO_2) (Foley, 2011; Luth, 2014). Oxygen fugacity in peridotite xenoliths from ≥200 km depths (Fig. 1a) can vary from 4 to 1 log units below the fayalite-magnetite-quartz (FMQ) equilibrium (Goncharov, 2012; Stachel and Luth, 2015; Stagno etal., 2013; Yaxley etal., 2012). Low fO_2 can maintain stability of hydrocarbon (HC) species in the fluid phase (Foley, 2011; Luth, 2014; Stachel and Luth, 2015; Griffin et al., 2018). Numerous experiments under mantle *P-T-*fO_2 conditions studied the compositions of reduced fluids that contain HCs (Huizenga etal., 2012; Kolesnikov etal., 2017; Lobanov etal., 2013; Matveev etal., 1997; Sokol etal., 2009, 2017a, 2017b; Taylor and Green, 1988) and N-bearing species. The results show that ultra-reduced quenched fluids at upper mantle pressures and temperatures consist of light alkanes (CH_4, C_2H_6, C_3H_8 and C_4H_{10}), water, and hydrogen (Huizenga etal., 2012; Matveev etal., 1997; Sokol etal., 2009; Taylor and Green, 1988). Gas chromatography-mass spectrometry (GC–MS) reveals more than thirty HC species in quenched fluids synthesized at fO_2 near IW(Sokol etal., 2017a). However, bulk carbon in the recovered fluid phase decreases dramatically as oxygen

* Corresponding author.
E-mail address: sokola@igm.nsc.ru (A.G. Sokol).

https://doi.org/10.1016/j.lithos.2018.08.025
0024-4937/

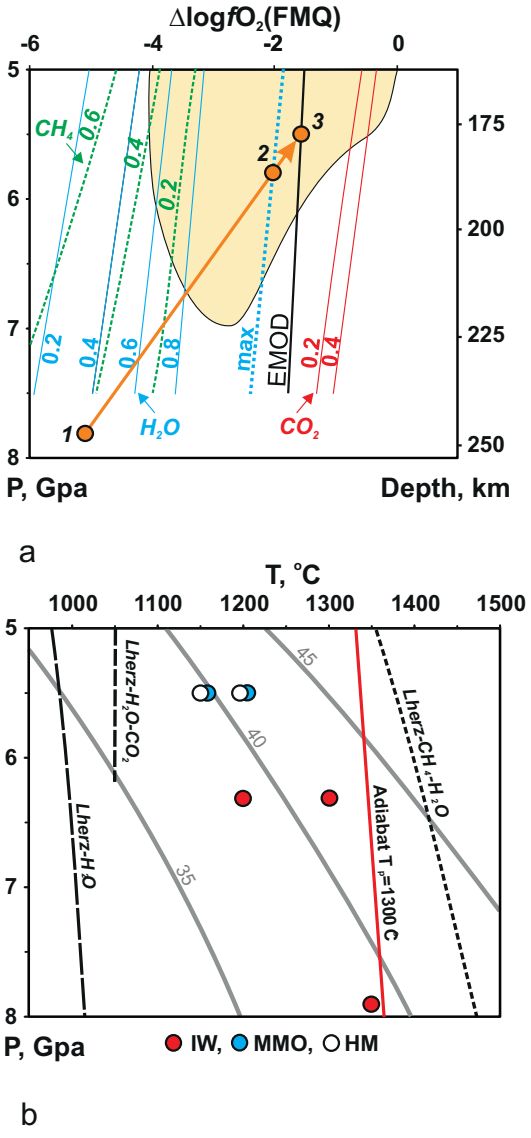

Fig. 1. P-T-fO_2 parameters of experiments and available data on upper mantle temperatures and oxygen fugacity. (a)Pressure-Δlog fO_2 (FMQ) diagram from Stachel and Luth (2015) illustrating redox conditions and speciation changes in C-H-O fluids along the 40 mW/m^2 geotherm (Hasterok and Chapman, 2011). *Brown field* covers P-fO_2 range inferred for deepest mantle xenoliths; blue lines show the calculated molar fraction of H_2O; *green dash lines* show the molar fraction of CH_4; *thin red lines* are the molar fraction of CO_2. EMOD is the enstatite-magnesite-olivine-diamond buffer; (b)P-T conditions applied in this study. *Circles* mark runs with fH_2 buffered by IW (Fe-FeO), MMO (Mo-MoO_2) and HM (Fe_3O_4-Fe_2O_3) equilibrium; *heavy grey lines* are continental geotherms (heat flux values in mW/m^2); *red line* is mantle adiabat for a potential temperature of 1300 °C according to Hasterok and Chapman (2011); *dashed lines* are lherzolite solidi: water saturated solidus (Green, 2015), in the presence H_2O-CO_2(Dvir and Kessel, 2017) and CH_4-H_2O at IW-buffered fO_2(Litasov etal., 2014). *Numerals* 1–3 and *arrow* indicate estimated P-fO_2 parameters of three main stages of fluid-rock interaction during ascent of fluids through peridotitic mantle (this study).

fugacity increases to +2.5 Δlog fO_2IW, or near the carbon-saturated maximum H_2O content for C-O-H fluids (CW). These fluids almost lack methane and contain about 1 rel.% of C_2-C_4 alkanes, as well as trace amounts of other alkanes, alcohols and carboxylic acids (Sokol etal., 2017a). Nitrogen speciation likewise changes at higher oxygen fugacity: NH_3 is the main nitrogen host in N-rich ultra-reduced mantle fluids (LiandKeppler, 2014; Sokol etal., 2017b) but it becomes commensurate with N_2 already at fO_2 of about IW(Sokol etal., 2017b). In low-N reduced fluids, most nitrogen resides in methaneimine (CH_3N) (Sokol etal., 2017a).

Mantle fluids occupy interstitial spaces in silicate rocks. Therefore, it is reasonable to expect fluid-rock interactions to influence fluid composition. To date, only recent models (Mikhail and Sverjensky, 2014; Sverjensky etal., 2014) have considered the fluid phase as a product of such interaction. Sverjensky etal. (2014) used a specially designed Deep Earth Water theoretical model to investigate the compositions of fluids in equilibrium with eclogite and peridotite at $P \leq 6.0$ GPa and temperatures typical of subduction settings (600–1000 deg C) and subcontinental lithospheric mantle (600–1200 deg C). They concluded that fluids equilibrated with diamond and eclogite minerals in subducting slabs contained significant amounts of dissolved ionic organic carbon-bearing species, especially acetic acid and acetate ($C_2H_3O_2^-$), whereas dissolved molecular species of carbon (mainly CO_2 or CH_4) were present in fluids equilibrated with peridotite. Note that the components of mineral systems are natural analogs of classical catalytical systems used in industrial technologies of HC synthesis and thus may catalyze reactions between volatiles. As demonstrated by Foustoukos and Seyfried (2004), Fe- and Cr-bearing minerals can catalyze the formation of hydrocarbons by Fischer-Tropsch type (FTT) reactions. The same property is known for Fe-Ni alloys (Horita and Berndt, 1999; Palyanov etal., 2012) which are presumably stable at depths below 250 km (Rohrbach and Schmidt, 2011). As metallic iron, Fe-Ni alloy, iron carbide and nitride have been found as inclusions in mantle diamonds and silicates (Jacobetal., 2004; Kaminsky and Wirth, 2011, 2017; Smith etal., 2016; Sobolev etal., 1981; Stachel etal., 1998), experimental research of fluid compositions in the peridotite-C-O-H-N system at upper mantle P-T-fO_2 conditions is of special interest.

This comprehensive study focuses on fluid-lherzolite interactions under typical upper mantle *P-T-*fO_2 conditions, and the ensuing composition changes to the fluid, silicate and metal phases of lherzolite. Recovered fluids in the lherzolite-C-O-H-N system at 5.5–7.8 GPa, 1150–1350 deg C, and fO_2 from 2.5 log units below to 3.5 log units above IW are analyzed using gas chromatography–mass spectrometry (GC–MS). The pressures and temperatures, as well as a part of the fO_2 range used in quenching experiments, correspond to values reported for the deepest mantle xenoliths from kimberlites (Fig. 1a) (Goncharov, 2012; Stachel and Luth, 2015; Stagno etal., 2013; Yaxley etal., 2012). More reduced experimental conditions represent those inferred for Fe^0-saturated (Rohrbach and Schmidt, 2011) and early Earth's (Yang etal., 2016) mantle.

2. Methods

2.1. Starting materials

Experimental charges consisted of synthetic K-free lherzolite (Lz1) or natural K-bearing lherzolite (Lz2) samples (Table 1). To provide iron saturation, 3 wt.% Fe^0 was added to a K-free mixture of oxides reproducing the composition of Lz. The same composition was used in experiments by Litasov etal. (2014). The charges included powdered graphite (>50 wt.% of the sample, Alfa Aesar, 99.9999% pure) which was pre-dried at 110 deg C for 30 days and contained CO_2 and H_2O, 700 ppm each (Sokol etal., 2017a). Part of the graphite was used to protect the capsule walls from contact with metallic iron stored in Lz1 (Supplementary Fig. S1) and the other part was carefully mixed with Lz1 and placed at the charge center. Graphite-saturated fluids with variable ratios of hydrogen to oxygen and nitrogen were synthesized using chemical-grade docosane ($C_{22}H_{46}$), stearic acid ($C_{18}H_{36}O_2$), and melamine ($C_3H_6N_6$), with some air captured during capsule assembly. The melamine-free charges, with a volumetrically measured porosity reaching 39 ± 2.5 vol%, contained 0.01 to 0.02 wt.% N. K-bearing lherzolite (Lz2) was a powdered garnet-bearing lherzolitic xenolith Uv-419/09 (with 4.5 wt.% clinopyroxene) from the Udachnaya kimberlite (Doucet etal., 2013), but the prepared Lz2 powder slightly differed

Table 1
Major-element compositions of starting lherzolites and magnesite (wt%).

	Lz1	Lz2	Magnesite
SiO_2	44.2	44.6	–
TiO_2	0.29	0.07	–
Al_2O_3	3.46	1.67	–
Cr_2O_3	0.69	0.49	–
FeO	10.7	7.99	–
MnO	–	0.11	–
NiO	0.29	0.23	–
MgO	37.1	42.64	43.35
CaO	2.96	1.43	4.95
Na_2O	0.39	0.32	–
K_2O	–	0.41	–
Total	100.1	100.0	48.3

Lz1 mixture of oxides; iron saturation was provided by. adding 3 wt% Fe^0(Litasov etal. (2014);
Lz2 garnet-bearing lherzolitic xenolith Uv-419/09. (Doucet etal., 2013);
Magnesite– natural magnesite from Satka deposit.(Ural region, Russian Federation).

from the xenolith composition reported by Doucet etal. (2013) in that it was mixed with stearic acid ($C_{18}H_{36}O_2$) or with natural magnesite (in two out of four runs), without graphite (Table 2). No Fe^0 was added to the Lz2 charges. In a test run (#2048_2_3), the charge consisted of Lz2 and distilled water only, and the quenched fluid was not analyzed. The fluid-generating materials were placed on the bottom of Pt or Au capsules (2.0 or 3.0 mm outer diameters; 0.2 mm wall thickness) (Supplementary Fig. S1), which were then sealed and arc-welded.

The temperature range selected for the 5.5, 6.3, and 7.8 GPa experiments was below the solidus of the Lz1-C-O-H system studied by Litasov etal. (2014), with fO_2 at the Mo-MoO_2 (MMO) and Fe-FeO (IW) equilibria (Fig. 1b). Thus, the P-T-fO_2 range in our reduced experiments was expected to provide interactions between the subsolidus fluid, assemblages of solid silicate phases, and the metal phase. The effect of fluids that formed at 5.5 GPa during HC oxidation on the solidus of the Lz2-C-O-H system was investigated with reference to the lherzolite solidus in the presence of H_2O and H_2O-CO_2 fluids reported by Green (2015) and Dvir and Kessel (2017).

2.2. High-pressure experiments

Experiments at 5.5, 6.3 and 7.8 GPa were carried out in a split-sphere multi-anvil high-pressure apparatus (Palyanov etal., 2010). Pressure was calibrated by recording the change in the resistance of Bi at 2.55 GPa and PbSe at 4.0 and 6.8 GPa at room temperature and at 1350 deg C by bracketing the graphite-diamond equilibrium (Day, 2012) in the $Ni_{0.7}$-$Fe_{0.3}$-C system. Temperature was monitored in each run with a $PtRh_6$/$PtRh_{30}$ thermocouple calibrated at 6.3 GPa using the melting points of Al, Ag (Sokol etal., 2015a). Pressures and temperatures were measured with an accuracy of ± 0.1 GPa and ± 20 deg C, respectively (Palyanov etal., 2010; Sokol etal., 2015a).

We applied the double-capsule technique (Sokol etal., 2009) for IW and MMO buffering of fH_2, with inner capsules placed into thick-walled Mo or Fe outer capsules (Supplementary Fig. S1). Hydrogen was generated by the reaction of water (15 mg H_2O, released by talc decomposition) with Fe or Mo from the outer capsule. The flow of hydrogen between the outer and inner capsules maintained stable fH_2 in the charge. The outer capsule was checked after each run for the presence of both metal and metal oxide. In a special series of 40-h and150-h runs with the Fe_2O_3-Fe_3O_4 (HM) external buffer, reduced C-O-H-N fluids underwent oxidation due to hydrogen diffusion from the high fH_2 environment composed of the sample + initial fluid through the inner capsule walls to the low fH_2 environment of the HM buffer. This led to an fO_2 increase to the EMOD (enstatite-magnesite-olivine-diamond) equilibrium inside the capsules. In these experiments, Pt or Au capsules were placed in containers made of a compressed Fe_2O_3 + CsCl water-free mixture with a weight ratio of 2:1 (Sokol etal., 2015b). According to XRD, Fe_2O_3 from the outer container partly reduced to a mixture 1:1 and 1:4 of Fe_2O_3 and Fe_3O_4 phases after 40 h and 150 h runs, respectively. As shown by our previous calculations for quenched C-O-H-N fluids (Sokol etal., 2017b), their fO_2 may generally vary from −2.5 Δlog fO_2 IW to +2.5 Δlog fO_2IW depending on the initial H_2O contents in the charge and the selected IW or MMO buffers for fH_2. Note that the MMO buffer is slightly more oxidized (+1 Δlog fO_2 IW) (Litasov etal., 2014; Sokol etal., 2009). Additional use of outer Fe_2O_3 containers extended the fO_2 range in the inner capsule with Lz2 to the more oxidized conditions of the EMOD equilibrium or + 3.5 Δlog fO_2IW.

Runs with low fO_2 in the Lz1-C-O-H-N system lasted 10 h in most cases (Table 2). A duration of at least 2 h was required for the formation of an equilibrated HC-bearing fluid in the C-O-H-N system at 6.3 GPa and 1150–1350 deg C (Sokol etal., 2017a, 2017b). Judging by the formation of unzoned crystals of silicates in 10 h runs (Fig. 2), the Lz1-C-O-H-N system, with the given fluid content, attained equilibrium even in the lowest-temperature runs. Run durations in the lherzolite melting experiments by Litasov etal. (2014) were from 4 to 12 h. Prolonged durations of 40 to 150 h for the Lz2-C-O-H-N system and external fH_2 buffering at HM provided maximum oxidation of HCs and allowed insights into the composition of fluids re-equilibrated with carbonate-saturated lherzolite. Thus, the experimental run durations were sufficiently long, and the chemical environment sufficiently stable, to produce fluids presumed to be in equilibrium with the mineral assemblage present.

At the end of the experimental run, samples were quenched at 200 deg./s under isobaric conditions.

2.3. Gas chromatography-mass spectrometry

The composition of the quenched fluid was analyzed with a *Thermo Scientific Focus GC/DSQ II*MS analyzer (USA). Pt or Au capsules were placed into a crush cell connected on-line to the gas chromatograph before the analytical column and were heated to 120–130 deg C for 90 min in a stream of carrier gas at a pressure of 50 kPa (99.9999% pure He). As a result of heating, most components in the quenched fluids passed to the gas phase, whereby pressure in the capsules increased. Relatively low heating temperatures precluded changes in the speciation of the analyzed gases. The gas mixture was extracted from the capsules by crushing. Trace amounts of poorly volatile components of the quenched fluids, especially heavy hydrocarbons (>C_{18}), remained in the capsules. A blank run was performed to check whether gas emission from the capsule had stopped.

Relative concentrations (%) of volatiles in the analyzed mixtures were obtained by normalization: the total areas of all chromatographic peaks were normalized to 100%, and the areas of individual components defined their proportions in the mixture. The contents of water and principal organic volatiles in gaseous run products were quantified using calibration against external standards (Sokol etal., 2017b). Formethane-hexane alkanes, certified *Scotty Inc. NL*34522-PI and 34,525-PI gas standards were injected into the gas stream in the splitless mode. The quality of calibration was checked using the correlation coefficients R^2 in the relationships of peak area vs. injected gas amount: 0.9975 (16 *m/z*, $n = 22$) for methane, 0.9963 (26 + 30 m/z, $n = 16$) for ethane, 0.9986 (29 + 43 m/z, $n = 15$) for propane, and 0.9994 (29 + 43 *m/z*, $n = 17$) for butane. Calibration for water was either by injection of a known amount of deionised distilled water into the gas stream or by crushing of specially prepared Pt and Au capsules with H_2O. In the latter case, capsules of the same size as the experiments were filled with water, sealed, and welded following the standard procedure. The coefficient R^2 for H_2O was 0.9661 (18 m/z, $n = 7$). Analytical uncertainties for main species (H_2O, NH_3, and CO_2), expressed as precision, were < 10% and even <5% in most cases (in the range from 12.5 pptv to 12.5 ppbv); the uncertainty for C_1-C_4 alkanes was below 5%.

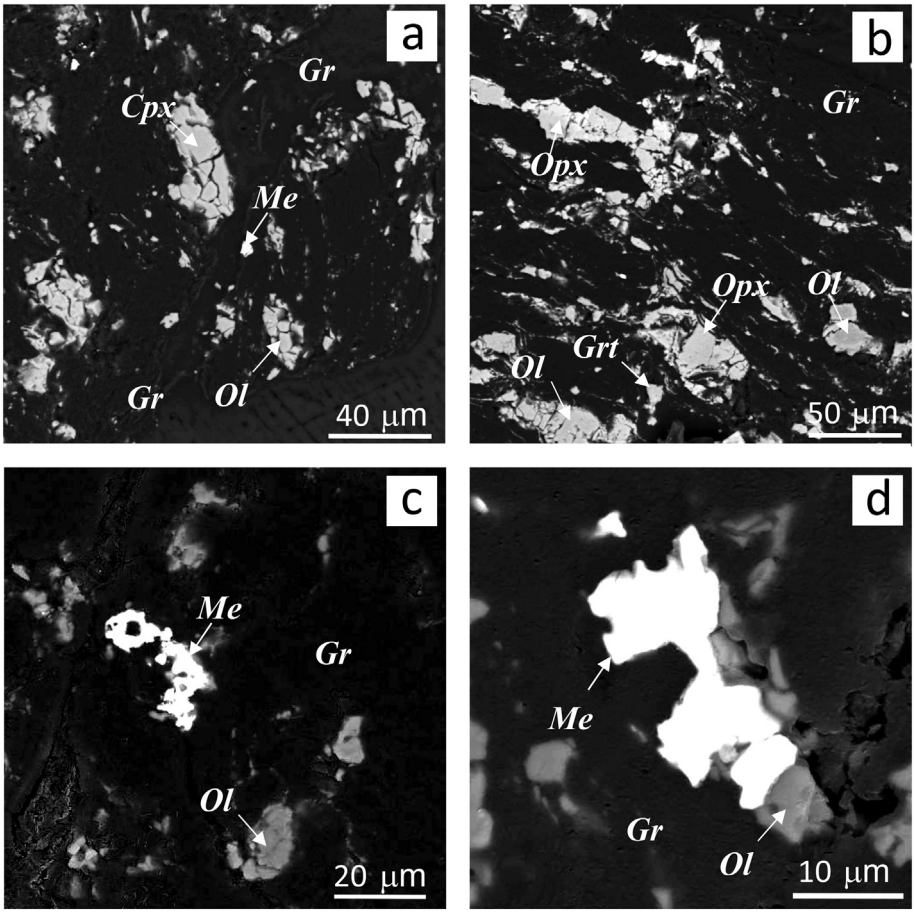

Fig. 2. Representative assemblages of silicate and metal phases after experiments with Lz1, SEM images. (a)run #1962_2_3, 6.3GPa, 1300°C (IW); (b)run #1969_2_3, 5.5 GPa, 1150°C (HM); (c)run #1956_2_1, 7.8 GPa, 1350°C (IW); (d)run #1985_2_2, 6.3 GPa, 1200°C (IW). Samples (dark grey to black) mainly consist of graphite; mineral names are abbreviated as Ol = olivine; Opx = orthopyroxene; Cpx = clinopyroxene; Grt = garnet; Me = metal phase.

GC–MS measurements were applied to the recovered aqueous fluid + vapor portion of the quenched fluids. These samples represent the speciation of fluids present in the charge at high P and T only in the absence of back reactions during quenching, which depend on coolingrates. Studies of cooling rate variations from 0.3 to 120 deg./s as a control of C–O–H fluid compositions at 2.4 GPa and 1000 deg C (Matveev etal. (1997), showed that C-O-H system re-equilibration stopped at <800 deg C. Fluids cooled at slower rates contained less hydrogen (2 to 4 mol%) and, correspondingly, more CH_4; the back reaction $C_2H_6 + H_2 \rightarrow 2CH_4$ stopped completely only when cooling was at 120 deg./s. In our earlier study of composition changes in C-O-H fluids as a function of cooling rates, in 15 h-long runs at 6.3 GPa and 1600 deg C (Sokol etal., 2009), CH_4 and C_2H_6 increased from 2 to 3 to 9–10 mol% and from 1 to 3 mol%, respectively, as cooling slowed from 200 to 27 deg./s; further deceleration to 1 deg./s did not change the concentration of CH_4, but led to a C_2H_6 increase from 3 to 4–5 mol% (Sokol etal., 2009). Synthesis of hydrocarbons most likely was due to back reactions of hydrogen with graphite during slow cooling. In subsequent experiments with C-O-H-N fluids at 1400 deg C (Sokol etal., 2017b), we compared rapid quenching at 200 deg./s and slow cooling at 1 deg./s (200 times slower) and observed a ten-fold increase (from ~0.01 to ~0.1) in C_{15-19} alkanes and formation of minor amounts (≤0.5 rel.%) of olefins, arenes, and oxygenated hydrocarbons (0.2 rel.% acetic acid and higher concentrations of C_{10}, C_{13} and C_{15} acids). A similar increase in heavy HCs at slow cooling rates was also reported by Kolesnikov etal. (2017). Concentrations of NH_3 and N_2 species in O-H-N fluids are likewise sensitive to cooling rates (Li and Keppler, 2014), but nitrogen speciation in fluids does not change at faster cooling of 140 deg./s instead of 70 deg./s. Thus, quenching from 1100 to 1400 deg C to room temperature at 200 deg./s can impede back reactions in the C-O-H-N system and furnish reliable evidence of fluid compositions at the applied *P–T* conditions. Possible minor H_2 loss by diffusion between the quenching and analysis time had no influence on the contents of species because their reactions were “frozen”.

Unfortunately, Mg-, Si- and Na-bearing species that were potentially present in H_2O-rich fluids may have remained irresolvable by GC–MS as they became unstable during quenching. In an earlier study of the Mg_2SiO_4-H_2O-C system (Sokol and Pal'yanov, 2008), we obtained a quenched solute from a fluid which consisted of coesite, enstatite, and amorphous SiO_2 but lacked hydrated material. Thus we infer that no part of the water content entered the solid phases upon quenching and all water was analyzed by GC–MS after the capsule was opened.

2.4. EDS and EMPA

Samples from capsules opened by crushing in the GC–MS analyzer were most often crumbly and the pieces were impregnated with epoxy resin in a vacuum. After resin polymerization, the samples were polished under kerosene, without the use of water (final polishing stage 1 μm Al_2O_3). Note that the amount of Lz1 in the samples (≤3.6 mg, or < 50 wt.%) was relatively small, and it was difficult to collect a significant quantity of silicate and metal grains on the polished surface (Fig. 2).

Preliminary examination of samples by optical (*Carl Zeiss Stemi 2000-C*) and scanning electron (*Tescan MYRA 3 LMU*) microscopy revealed a metal phase besides silicates in some samples. Its composition was studied by electron microprobe analysis (EMPA) using a *Jeol JXA-8100* microanalyzer, after 10 nm gold sputtering, at 15 kV accelerating

voltage, 200 nA beam current, and 1 to 2 μm beam diameters. However, heating of small grains in a loose aggregate of silicates and graphite led to a decrease in beam current and resultant instability. For this reason, the metal phase composition was also analyzed using a *Tescan MYRA 3 LMU* scanning electron microscope coupled with an INCA EDS microanalysis system 450 with an Oxford Instruments liquid nitrogen-free Large area EDSX-Max-80 Silicon Drift Detector. The instruments were operated at an accelerating voltage of 20 keV, a beam current of 1 nA, and a spot diameter of ~10 nm; the counting time for spectra collection was 60 s. The EDS spectra were optimized for quantification using the standard XPP procedure included in the *INCA Energy 450* software. Where possible, analyses were made on >10 μm metal grains. Noise from the host graphite deteriorated the quality of quantitative analyses for carbon.

Silicate and carbonate phases were analyzed with a *Jeol JXA-8100* analyzer at 20 kV accelerating voltage, 20 nA beam current, and 1 to 2 μm beam diameter. The acquisition time for each element was 15 s. Standards used were: pyrope (O-145) for Si, Al and Fe; Cr-garnet (Ud-92); Mn-garnet (Mn-IGEM); diopside for Mg and Ca; albite for Na; orthoclase for K; ilmenite for Ti; and spinel for Ni. The uncertainty of the measurements was within 2 relative percent for all components.

2.5. Micro-Raman spectroscopy

Micro-Raman spectra were measured on a *Horiba Jobin Yvon LabRAM HR800* spectrometer equipped with an *Olympus BX41* microscope. A 532 nm solid state laser was used as an excitation source. The spectra were collected using an Olympus BX41 microscope equipped with an Olympus Plan 100× objective lens.

3. Results

In one series of experiments, fluids were synthesized in the metal-bearing Lz1-C-O-H-N system (Tables 2-4) and had either N-poor or N-rich compositions, with nitrogen captured as N_2 from minor amounts of air by the capsule assembly in the former case (0.01 to 0.02 wt.% N) and as NH_3 from melamine ($C_3H_6N_6$) added to the charge in the latter case (0.97 to 5.13 wt.% N). The charges contained either nominally oxygen-free docosane ($C_{22}H_{46}$) or oxygen-bearing stearic acid ($C_{18}H_{36}O_2$) as a source of hydrocarbons (Table 2) within each group. Another series of experiments was applied to the system with Lz2, and the charges additionally contained stearic acid ($C_{18}H_{36}O_2$) or magnesite (in some runs) (Table 2). This diversity of charge compositions, together with the use of three fH_2 buffers (IW, MMO and HM) and long run durations, allowed us to obtain a range of ultra-reduced to moderately oxidized fluid compositions. All fluids were equilibrated with lherzolite at 5.5–7.8 GPa and 1150–1350 deg C (Figs. 2, 3). Oxygen fugacity (fO_2) was estimated with reference to metal and magnesite saturations of lherzolite, as well as CO_2 concentrations in the fluid phase, because its calculation for the system including >100 fluid species was problematic.

3.1. Solid phases

3.1.1. Lz1-C-O-H-N system

Sample charges of the Fe^0-bearing system yielded only fine (1 to 50 μm) silicate grains (Fig. 2; Table 1). Although the opening of capsules by crushing for GC–MS analysis damaged the samples, the phase composition of lherzolite could be reconstructed from EDS and EMPA data (Tables 2, S1). Four-phase assemblages (Ol+Opx + Cpx + Grt) in equilibrium with both reduced and relatively oxidized fluids were observed over the whole *P-T* range. Assemblages of two or three minerals, missing one of pyroxenes and/or garnet, were found in samples with the fluid fraction exceeding 0.2. All analyzed samples with four-phase assemblages comprised a fluid phase and some also contained a metal phase. All mineral phases were homogeneous and unzoned. No traces of quenched melt were found in the run products, even when the fluid fraction was 0.2 to 0.4 (Table 2). Importantly, no quenched solute was detected, which indicated relatively low solubility of silicate components in the fluids. Some quenched solute was possibly present,

Table 2
Initial compositions of lherzolite-C-O-H-N systems, run parameters, and synthesized phase compositions.

Run #	Initial composition (mg)							Fluid fraction	N in charge (wt%)	Capsule	fH_2	P (GPa)	T (°C)	τ (hr)	Phase composition
	Graphite	$C_{22}H_{46}$	$C_{18}H_{36}O_2$	$C_3H_6N_6$	$MgCO_3$	H_2O	Lherzolite								
Lz1 + Fe^0															
1969_2_2	6.1	0.7	–	0.2	–	–	3.6	0.20	1.26	Pt	HM	5.5	1150	40	Ol, Opx, Cpx, Grt, Fl
1969_2_3	6.2	–	0.8	–	–	–	3.6	0.18	0.02	Pt	HM	5.5	1150	40	Ol, Opx, Grt, Fl
1969_2_4	6.9	–	0.7	0.2	–	–	3.7	0.20	1.16	Pt	HM	5.5	1150	40	Fl*
1968_2_3	11.4	0.8	–	–	–	–	3.6	0.18	0.01	Pt	MMO	5.5	1150	10	Ol, Opx, Cpx, Grt, Me, Fl
1968_2_4	12.6	0.6	–	0.25	–	–	3.8	0.18	0.97	Pt	MMO	5.5	1150	10	Ol, Cpx, Grt, Fl
996_5_1	8.1	0.7	–	–	–	–	3.8	0.16	0.02	Pt	MMO	5.5	1200	10	Ol, Opx, Cpx, Fl
996_5_2	8.5	0.6	–	0.2	–	–	3.7	0.18	1.03	Pt	MMO	5.5	1200	10	Ol, Opx, Cpx, Me, Fl
1985_2_1	7.4	0.7	–	–	–	–	3.6	0.16	0.02	Au	IW	6.3	1200	10	Ol, Opx, Cpx, Me, Fl
1985_2_2	7.7	0.7	–	0.2	–	–	3.8	0.19	1.08	Au	IW	6.3	1200	10	Ol,Opx, Cpx, Grt, Me, Fl
1985_2_3	7.4	–	0.7	–	–	–	3.5	0.17	0.02	Au	IW	6.3	1200	10	Ol, Cpx, Grt, Fl
1985_2_4	7.8	–	0.7	0.2	–	–	3.6	0.20	1.08	Au	IW	6.3	1200	10	Ol, Opx, Cpx, Grt, Me, Fl
1959_2_4	8.4	–	–	0.7	–	–	1.3	0.35	4.49	Pt	IW	6.3	1300	10	Ol, Opx, Cpx Grt, Me, Fl
1959_2_5	8.3	–	0.7	–	–	–	1.3	0.35	0.02	Pt	IW	6.3	1300	10	Ol, Opx, Fl
1962_2_2	6.9	–	0.7	–	–	–	3.6	0.16	0.02	Pt	IW	6.3	1300	10	Ol, Opx, Grt, Fl
1962_2_3	7.3	0.6	–	0.2	–	–	3.6	0.18	1.14	Pt	IW	6.3	1300	10	Ol, Cpx, Me, Fl
1962_2_4	10.2	–	0.6	0.3	–	–	3.6	0.20	1.36	Pt	IW	6.3	1300	10	Ol, Opx, Cpx, Grt, Fl
1956_2_1	8.3	–	–	0.8	–	–	1.3	0.38	5.13	Pt	IW	7.8	1350	10	Ol, Grt, Me, Fl
1956_2_2	9	–	0.8	–	–	–	1.2	0.40	0.02	Pt	IW	7.8	1350	10	Ol, Opx, Fl
1987_2_1	9.4	0.7	–	–	–	–	4.3	0.14	0.01	Pt	IW	7.8	1350	10	Ol, Opx, Cpx, Grt, Me, Fl
Lz2 ± $MgCO_3$															
542_8_3	–	–	1.2	–	5.2	–	27.4	0.04	0.02	Pt	HM	5.5	1200	40	Ol, Opx, Cpx, Grt, Mgs, Fl
2048_2_1	–	–	0.5	–	2.5	–	11.5	0.04	0.02	Au	HM	5.5	1200	150	Ol, Opx, Cpx, Grt, Mgs, L, Fl
2048_2_3**	–	–	–	–	–	0.4	15.1	0.02	<0.02	Au	HM	5.5	1200	150	Ol, Opx, Cpx, Grt, L
2048_2_4	–	–	0.4	–	–	–	14.9	0.03	0.02	Au	HM	5.5	1200	150	Ol, Opx, Cpx, Grt, Mgs, Fl

Fluid fraction is weight fraction of fluid-generating material in the charge without graphite and magnesite. N content in the charge is calculated with regard to graphite; in runs without melamine, nitrogen contents were calculated proceeding from air N_2 at 39% measured average porosity of the charge.
Me is iron-rich metal phase, L is quenched melt; Fl is quenched fluid; *analysis of silicate phase composition was not possible. **- quenched fluid not analyzed.

Table 3
Composition of quenched fluid in lherzolite-C-O-H-N systems (rel. %).

Run #	Alkanes	Olefins	Arenes	Furans	Alcohols, ethers	Aldehydes	Ketones	Carboxylic acids	N_2	CH_3N	H_3N	H_2O	CO_2	Total nitrogen*
1968_2_3	91	0.3	0.1	0.2	0.4	0.5	0.3	0.2	0.1	4.4	0.5	2.3	<0.1	2.6
1968_2_4	14	0.6	0.2	0.3	1.1	0.8	0.8	0.8	46	0.4	22	13	0.2	57
1969_2_2	0.5	0.1	–	–	0.3	0.3	0.1	0.2	84	<0.1	1.0	5.4	7.8	85
1969_2_3	7.5	1.2	0.6	0.4	4.3	1.1	1.1	3.6	4.4	0.1	0.2	66	8.7	4.8
1969_2_4	1.0	0.5	0.1	0.1	0.4	0.7	0.6	0.8	57	<0.1	0.5	18	19.7	57
996_5_1	91	0.4	0.1	0.1	0.4	0.5	0.3	0.2	0.1	1.9	1.2	3.5	<0.1	1.7
1985_2_1	81	0.3	0.1	0.1	0.5	0.4	0.3	0.9	<0.1	2.3	6.6	7.7	<0.1	4.6
1985_2_2	4.6	0.4	0.2	0.2	0.6	0.7	0.3	1.1	0.4	0.1	60	31	0.3	31
1985_2_3	4.5	1.4	0.7	0.6	10	3.0	1.7	4.0	0.4	0.2	0.3	72	0.1	0.7
1959_2_4	13	1.3	0.4	–	0.9	3.6	4.5	1.2	33	0.3	25	13	2.2	46
1959_2_5	3.2	1.2	0.2	0.3	2.0	3.2	1.1	4.5	0.2	0.1	0.3	81	1.5	1.2
1962_2_2	12	0.2	–	–	0.7	0.5	0.5	0.1	0.1	0.3	0.1	85	<0.1	0.4
1962_2_3	25	–	–	–	0.1	0.1	0.1	0.1	17	0.6	33	24	<0.1	34
1962_2_4	4.7	0.1	–	–	0.1	0.1	0.1	0.0	6.4	0.1	78	11	<0.1	45
1956_2_1	3.5	0.9	–	0.4	3.3	3.8	1.5	2.6	27	0.5	41	13	0.8	49
1956_2_2	4.5	1.2	0.4	0.3	0.8	1.4	1.5	1.9	0.3	0.1	0.7	85	0.4	1.0
1987_2_1	43	0.4	0.1	–	0.8	1.7	0.6	0.6	0.2	0.4	3.0	47	1.6	2.0
542_8_3	10.5	<0.1	–	–	0.8	0. 3	0.1	0.2	1.1	0.1	2.2	82	2.1	2.6
2048_2_1	2.6	0.3	0.1	0.2	1.5	1.5	0.4	2.5	42	0.5	1.3	43	3.3	43.6
2048_2_4	1.7	1.3	0.2	0.3	2.6	3.6	1.8	2.8	41	0.81	0.9	36	5.5	42.1

After runs # 996_5_2 and 1985_2_4, the capsule was unsealed during GC–MS analysis.
* bulk nitrogen in the fluid normalized to N_2 with regard to all N-bearing species.

especially in H_2O-rich samples, but its characteristic textures may have been partly destroyed during GC–MS analysis.

Olivine in the lherzolite matrix was typically anhedral, ~1–50 μm in size. Olivine coexisting with the metal phase had Mg# (molar MgO/(MgO + FeO) × 100) 91–95 and contained up to 0.2 wt.% NiO (Fig. 4a; Table S1). Olivine with the highest Mg# of 95 also was found in samples with reduced fluid where no metal phase was identified by EDS. In contrast, olivines from H_2O-rich and metal-free samples had the lowest Mg# (78–80) but were slightly richer in NiO (0.2–0.3 wt.%).

Orthopyroxene occurred as subhedral grains (up to 50 μm). It had Mg# 78–91 and contained ≤0.2 wt.% Cr_2O_3, 0.1–0.6 wt.% CaO, and 0.2–0.9 wt.% Al_2O_3. Orthopyroxene in metal-free samples had Mg# 78–83 (Fig. 4a), which was lowest in the sample with 66 rel.% H_2O and 9 rel. % CO_2. Clinopyroxene existed as subhedral grains (up to 30 μm) and approached a diopside composition with Ca# (molar CaO/(CaO +MgO) × 100) from 45 to 50 and 0.1–1.8 wt.% FeO. Concentrations of Na_2O and Al_2O_3 in clinopyroxene decreased from 1.7 and 4.5 wt.% (Litasov etal., 2014) to zero (Supplementary Fig. S2; Table S1) as the fluid fraction in the Lz1-C-O-H-N system increased from 0.08 to >0.2. Garnet occurred as isometric crystals, up to 10 μm, with 3.4–4.6 wt.% CaO, 0.5–4.6 wt.% Cr_2O_3, and 6.0–14 wt.% FeO.

Metal grains (≤ 30 μm in size) had irregular shapes and were hosted by a silicate matrix (Fig. 2c, d). They lacked the typical dendritic habit formed upon quenching of C– and N-rich metal melts (Sokol etal., 2017c). Nickel concentrations in the metal phase were ranged from 0.6 to 8 wt.% (Table 4), but reached 25 wt.% Ni in run #1985_2_4 with a H_2O-rich fluid. Another important feature of the metal phase was high nitrogen content (3–8.5 wt.%) in the case of melamine alone in the charge (Fig. 5; Table 4). However, nitrogen derived from captured air only was below the EDS detection limit.

Table 4
Composition of metal phase in the lherzolite-C-O-H-N system (wt%).

Run #	$C_3H_6N_6$ in charge	n	Fe	Ni	N	Total	C (calc)
1968_2_3	–	8	80 (2)	5 (1)	–	84.9	*15?*
996_5_2	+	7	84 (2)	5.9 (5)	6.5 (9)	96.5	3.5
1959_2_4	+	5	76 (1)	–	7.2 (8)	96.7	3.3
1956_2_1	+	6	85 (1)	0.6 (0.1)	8.5 (4)	93.7	6.3
1962_2_3	+	5	83 (1)	2.5 (1)	6.2 (1)	91.7	8.3
1985_2_1	–	5	82 (1)	6 (1)	–	87.7	*12.2?*
1985_2_2	+	6	78 (1)	8 (1)	4.1 (9)	94.2	5.8
1985_2_4	+	7	61 (2)	25 (2)	3 (1)	88.5	*11*

n is number of analyses; $C_3H_6N_6$ is melamine as source of nitrogen.
Numerals in parentheses show one sigma error, to last significant digit.

3.1.2. Lz2-C-O-H-N system

Experiments with the Lz2-C-O-H-N system yielded aggregates of large silicate and carbonate mineral grains. All samples consisted of olivine, orthopyroxene, clinopyroxene, and garnet (Fig. 3). Magnesite was present in HM-buffered fH_2 samples (Fig. 3). Soot-like carbon was found in the lower part of graphite-free capsules (Table 2). Sample fragments from crushed capsules showed no indication of melting.

Olivine occurred as subhedral crystals, sometimes prismatic, up to 400 μm, compositionally close to olivine in the starting lherzolite (Mg# 92–93) (Fig. 4b; Table S1). Orthopyroxene also occurred as subhedral prismatic crystals. Some orthopyroxene grains obtained in a 40-h run (# 542_8_3) were as large as 300 μm and had Mg# up to 98 (cf. Mg# 93 in orthopyroxene from the starting lherzolite), as a result of Fe loss from the sample to a non-cased Pt capsule. Orthopyroxene grains obtained in 150-h runs did not exceed 50–100 μm and were rimmed by clinopyroxene and/or magnesite (Fig. 3 d); those from an Au capsule had Mg# of about the starting value. Clinopyroxene occurred as subhedral prismatic or anhedral grains (50–200 μm). It contained higher MgO (Ca# 40–45) than the starting composition (Ca# 38), 1.1–2.3 wt.% FeO, and 0.3–0.5 to 2.3 wt.% Na_2O in charges with and without magnesite, respectively (Supplementary Fig. S2c). Garnet formed 50–150 μm isometric crystals and had the lowest FeO contents (2.1 wt.%) in Pt capsules with magnesite. Garnets from samples with magnesite synthesized in Au capsules had higher FeO (4.7 wt.%). A garnet composition almost the same as the starting one was obtained in a Au capsule without magnesite (Fig. 4b). Garnet synthesized in the Lz2-C-O-H-N system with magnesite contained more chromium (10–11.6 wt.% Cr_2O_3) than in magnesite-free runs (7.3 wt.% Cr_2O_3). These compositions plot on the lherzolite/wehrlite boundary (Supplementary Fig. S2a) in the CaO vs. Cr_2O_3 diagram (Sobolev etal., 1969). Minor composition changes in the main phases of lherzolite are due to its re-equilibration at slightly higher experimental pressures and temperatures than the parameters (5.0–5.1 GPa and 930–950 deg C) inferred from mineral geothermobarometry on the UV-419-09 xenolith (Doucetetal., 2013).

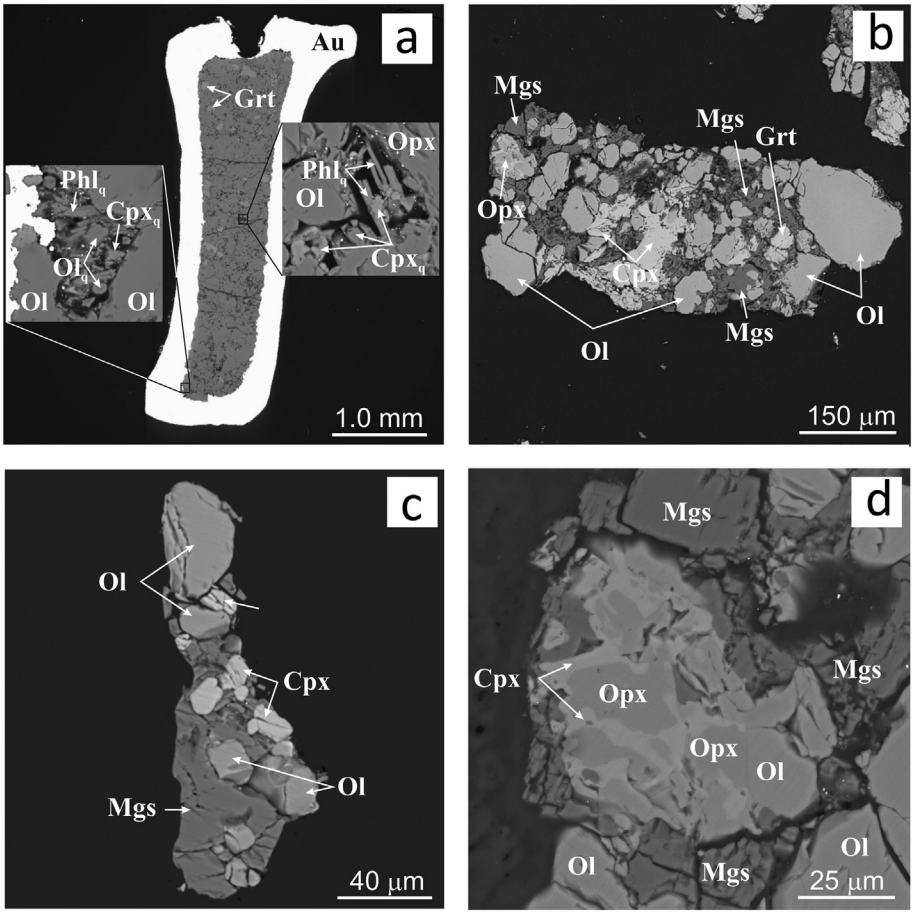

Fig. 3. Representative assemblages of silicate and carbonate phases after experiments with Lz2 at 5.5 GPa, 1200°C (HM), SEM images. (a)run #2048_2_3, test carbon-free sample with batches of hydrous silicate melt (mix of Phl_q, Ol_q and Cpx_q); (b)run #2048_2_1, magnesite-bearing sample; (c)run #542_8_3, magnesite-bearing sample; (d)fragment of sample from panel (b).

Garnet compositions had the same balance of two- and three-valent cations in the reduced and oxidized runs.

In the case of HM-buffered fH_2, carbonation of lherzolite was limitedby hydrogen diffusion from the high fH_2 environment of the sample + initial fluid composition to the low fH_2 environment of the external buffer. The process was facilitated during the replacement of olivine and orthopyroxene by magnesite and clinopyroxene (Fig. 2c, d)and remained incomplete even in 150-h runs 2048_2_1 and 2048_2_4. Recrystallized magnesite appeared as large anhedral crystals (up to 100 μm), in the runs where magnesite was originally present in the charge, or as small 10–20 μm grains, in run #2048_2_4 with a magnesite-free starting composition where it was produced by the reaction of CO_2 with olivine (Tables 2, S1). Recrystallized magnesite contained half of the starting CaO (2.6–2.8 wt.%) (Table 1) and 1.1–3.3 wt.% FeO, while newly-formed magnesite in run #2048_2_4 had less CaO (1.8 wt.%) but more FeO (4 wt.%).

A special study was made of microinclusions in large 300–400 μm olivines. According to Raman spectroscopy, the crystalline inclusions were magnesite in 40-h run #542_8_3 and aggregates of magnesite (bands 167, 297, 722 and 1094 cm^{-1}), calcite (band 1080 cm^{-1}) and graphite (band 1609 cm^{-1}) in 150-h run #2048_2_1 (Fig. 6). The shapes and compositions of inclusions in the latter run suggest that olivine captured dolomitic melt which quenched into an aggregate of magnesite, calcite, and graphite. Olivine from the xenolith used in the starting material for the experiments was free from carbonate inclusions (Doucet etal., 2013).

The composition of silicate phases in a test run with carbon-free Lz2-H_2O (#2048_2_3) was almost identical to that in run #2048_2_4 with stearic acid added to the charge (Tables 2, S1), but the intersertal texture between olivine and orthopyroxene crystals enclosed quenched hydrous silicate melt containing quench phlogopite and clinopyroxene (Fig. 3a). The melt composition reconstructed from EDS data (Table S1) was generally similar to that obtained by Litasov etal. (2014) at 6.0 GPa and 1300 deg C (with total oxides normalized to 100%), except for high K and Al, although these values should be treated as semi-quantitative, taking into account possible changes of melts during quenching and difficulty in determining melt compositions at small melt fractions.

3.2. Fluid phases

3.2.1. Metal-bearing Lz1-C-O-H-N system

Low-N fluids equilibrated with metal-saturated lherzolite in runs with IW and MMO hydrogen buffering contained 43 to 95 rel.% alkanes (Figs. 2, 7a, S3; Tables 2, 3, S2). These were mainly C_1-C_4 species (Fig. 8a), with high contents of CH_4 and C_2H_6 but <10 rel.% C_4H_{10}, while C_7-C_{18} alkanes were ≤ 0.5 rel.%. All other species were present in lower amounts, except for the 7.8 GPa and 1350 deg C run where the alkane contents were commensurate with H_2O. Alkenes (to 0.5 rel.%), aldehydes (to 1.7 rel.%), other oxygenated HCs (≤1.0 rel.%), and CO_2 (to 1.6 rel.%) were found in fluid with the highest H_2O content. Nitrogen mainly resided in NH_3 (to 6.6 rel.%) and CH_3N (to 4.4 rel.%) (Fig. 9a; Table S2). The same fluid composition was obtained in metal-free run #996_5_1. A metal phase was likely present in the sample but was outside the section analyzed.

N-rich fluids synthesized in the metal-saturated lherzolite-C-O-H-N system contained predominant NH_3, N_2, alkanes, and water (Figs. 9b,

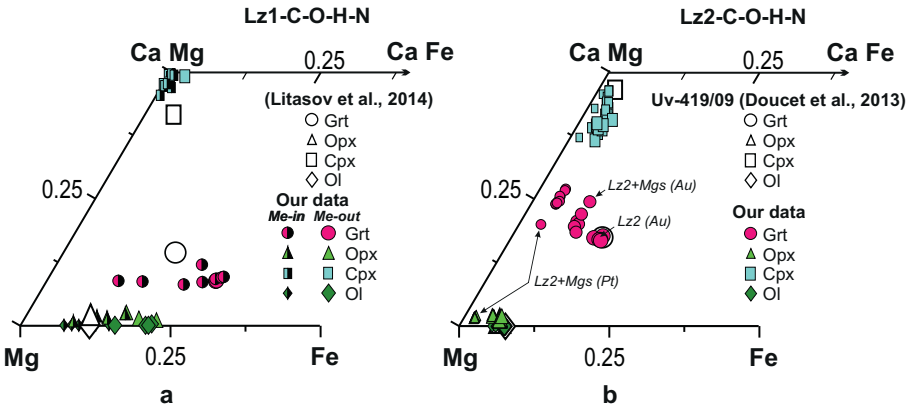

Fig. 4. Compositions of experimentally obtained olivine, orthopyroxene, garnet and clinopyroxene projected into the Mg–Fe–Ca space, compared with compositions of minerals in initial Lz1 and Lz2 according to Litasov etal., 2014 and Doucet etal. (2013), respectively. Lz2 + Mgs is charge Lz2 with magnesite. Me-in = metal-bearing sample, Me-out = metal-free sample. Au or Pt is inner capsule type.

10; Tables 3, S2). Fluid with the highest nitrogen contents in the case of solely melamine in the starting charge contained 60–77 rel.% NH_3, while N_2 did not exceed 6 rel.% and CH_3N was at the 0.1 rel.% level (Table 3). The N_2/NH_3 ratio varied from 0.01 to 4, remaining ≤1.3 in samples with the metal phase (Fig. 9b). Water was the second main fluid species (11 to 31 rel.%) and alkanes were within 5 rel.%. The fluid composition obtained from charges with a docosane+melamine mixture differed from that of docosane-free charges (Figs. 9b, 10; Tables 3, S2): the former had commensurate amounts of N hosts, with NH_3 much lower (13–33 rel.%) but N_2 notably higher (17–33 rel.%) than in the latter. The concentration of water was about the same (8–24 rel.%) as in the runs with melamine alone, while the concentration of alkanes increased to 14–25 rel.%. Nevertheless, at notably lower concentrations of HCs, the distribution of alkanes was the same as in N-poor fluids: predominant light alkanes and vanishing amounts of heavy alkanes. Metal-free run #1968_2_4 (Table 2) gave an N_2/NH_3 ratio of 2.1. Metal oxidation (likely partial) in the sample was possibly solely due to CO_2 and H_2O adsorbed on graphite. The charge in this run contained twice as much graphite than the other runs.

3.2.2. Metal-free Lz1-C-O-H-N system

Stearic acid was the main source of oxygen for Fe^0 oxidation in the charge. Quenched fluids in N-poor runs #1969_2_2, 1985_2_3, 1959_2_5 and 1962_2_2 with IW and MMO hydrogen buffering contained 66 to 85 rel.% H_2O (Fig. 7b; Table 3) and 3 to 12 rel.% of alkanes. Runs with reduced IW and MMO buffers yielded fluids with <1% of N-bearing species and N_2/NH_3 ratios from 0.5 (at 7.8 GPa and 1350 deg C) to 2.4 (at 6.3 GPa and 1200–1300 deg C). CO_2 in the fluids did not exceed 1.4 rel.%, whereas O-bearing HCs (alcohols, aldehydes, ketones, and carboxylic acids) reached significant amounts (10–19 rel. %). Fluids with higher H_2O contained less C_1-C_2 alkanes while higher alkanes had almost the same concentrations as in fluids with lower water content (Figs. 7, 8). The high-H_2O fluid synthesized at 6.3 GPa and 1200 deg C (run# 1985_2_3) had the highest concentrations of alcohols (e.g., 3 rel.% of methanol).

Run #1969_2_3 at 5.5 GPa and 1150 deg C, with a duration of 40 h and HM-buffered hydrogen, simulated oxidation of an HC-bearing fluid in the case of hydrogen diffusion from a Pt capsule. Partial oxidation of N-poor fluid led to an increase in CO_2 to 9 rel.% (Table 3), while HCs remained comparatively high: 7.5 rel.% alkanes and 10 rel.% oxygenated HCs, mainly, methanol and acetic acid (Supplementary Fig. S3b). Oxidation of N-rich fluid was simulated in two runs (#1969_2_2 and #1969_2_4) at 5.5 GPa and 1150 deg C, likewise with fH_2 at HM. Compositions were 57 to 84 rel.% N_2(Figs. 9b, 10), up to 18–20 rel.% H_2O and CO_2, within 1 rel.% NH_3 (N_2/NH_3 = 88 and 108), and a few percent of alkanes and oxygenated HCs (Table 2). Adsorbed gases were the only possible internal source of oxygen in metal-free runs #1969_2_2 (Table 2).

3.2.3. Lz2-C-O-H-N system

Fluids in carbonate-bearing Lz2 samples obtained in runs with HM-buffered fH_2 contained water and molecular nitrogen as main components (Figs. 8b, 11a; Table S2), moderate amounts of carbon species (1.7–10 rel.% alkanes, to 1 rel.% alkenes, and 1.3–11 rel.% oxygenated HCs), CO_2, and minor amounts of nitrogen-bearing species with high N_2/NH_3 = 10–90. As run duration increased from 40 h (run

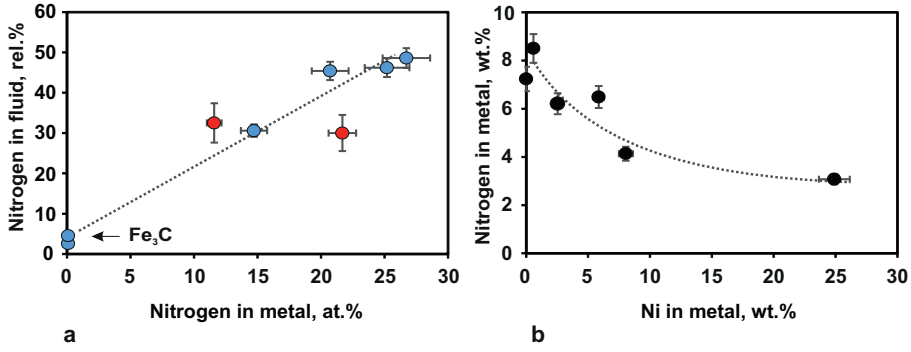

Fig. 5. (a)Effect of nitrogen contents in the fluid (calculated as N_2) on that in the metal phase (red colour shows compositions of metal phase from samples with nitrogen in fluid estimated from Supplementary Fig. S3); (b)decreasing N in the metal phase with increasing Ni.

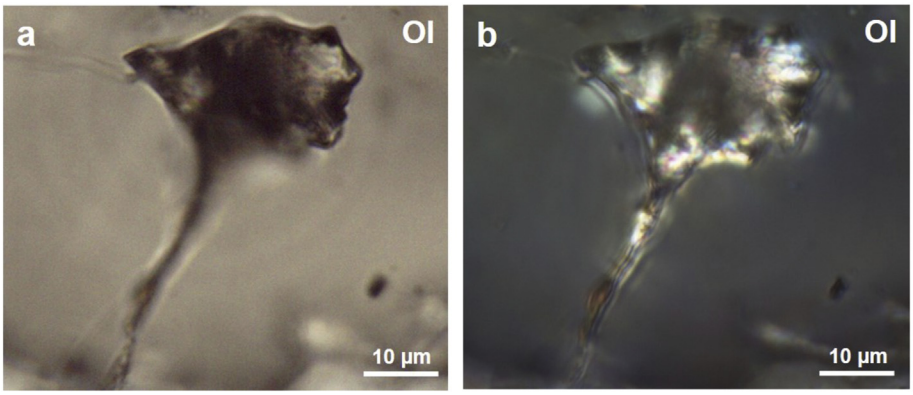

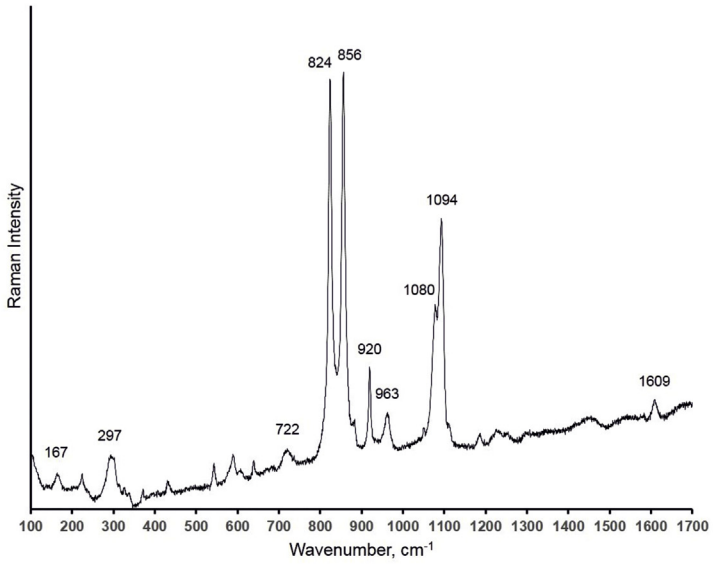

Fig. 6. Inclusion of quenched carbonate melt in olivine, 150-h run #2048_2_1 at P = 5.5 GPa and T = 1200°C, SEM images in transmitted (a)and polarized (b)light; (c)Raman spectrum of the inclusion: bands 824, 856, 920 and 963 cm^{-1} represent olivine (host); bands 167, 297, 722 and 1094 cm^{-1} are from magnesite; band 1080 cm^{-1} is from calcite; band 1609 cm^{-1} corresponds to graphite.

#542_8_3) to 150 h (runs #2048_2_1 and 2048_2_4), fluids changed toward lower H_2O (from 82 to 36 rel.%) but higher N_2 (1 to 42 rel.%) and CO_2 (2.1 to 5.5 rel.%) (Fig. 11a). The composition change resulted from diffusion of hydrogen which was consumed by the HM buffer. X-ray analysis of the buffer material after the runs revealed a mixture of Fe_2O_3 (~20% wt.%) and Fe_3O_4, which proves the workability of buffering in 150-h runs. The dramatic N_2 increase was due uniquely to a decrease in the amount of fluid. With a reasonable assumption that the charges captured identical amounts of air nitrogen, the amount of fluid in 150-h runs #2048_2_1 and 2048_2_4 can be inferred to have become 16 times less than in 40-h run #542_8_3. Hydrogen diffusion led to excess oxygen in the capsules which was spent on oxidation of HCs and C^0 produced by decomposition of stearic acid $C_{18}H_{36}O_2 \rightarrow 8CH_4 + 2H_2O + 10C^0$. Normalizing the fluid composition to nitrogen demonstrated that ≥97% of water was consumed in 150-h runs (Fig. 11 b), while the amount of CO_2 produced by oxidation reactions was slightly >10% of the amount of stearic acid added to the charges (Table 2). The presence of olivine, orthopyroxene, C^0 and magnesite maintained carbonation of lherzolite and held fO_2 at the EMOD equilibrium; the fluid was constantly re-equilibrated while water fugacity decreased. The process was evident in the presence of carbonate among the products of 150-h run #2048_2_4 with a magnesite-free starting charge. It is noteworthy that lherzolite became carbonated when CO_2 in the fluid reached 3.2–5.5 rel.% (Fig. 11b; Tables 2, S2), or slightly below the values predicted for the EMOD equilibrium (Stachel and Luth, 2015) as shown in Fig. 1a. Importantly, fluid in the Lz2-C-O-H-N system, with ultimately high EMOD-buffered fO_2, contained at least 9 rel.% C_2-C_{13} HC species (alkanes, alkenes, and O-bearing HCs) (Fig. 12a).

The fluid composition obtained in the test run with a carbon-free water-bearing charge (#2048_2_3) was not analyzed and remained unknown, but it obviously contained water, as it was released when the capsule was pierced after the run.

4. Discussion

4.1. Fluid composition

Strongly reduced N-poor fluids in the lherzolite-C-O-H-N system, over the entire applied *P-T* range, contain predominant lower alkanes (CH_4 and C_2H_6, $CH_4/C_2H_6 \leq 1$) but much less C_3H_8 and C_4H_{10}(Fig. 8a); the same HC species are found in N-rich reduced fluids (Fig. 11). Thermodynamic calculations (Huizenga etal., 2012; Litasov etal., 2014) predict slightly higher contents of CH_4 ($CH_4/C_2H_6 > 1$) in reduced C-O-H fluids. Fluid synthesized in runs #1969_2_2, 1985_2_3, 1959_2_5 and 1962_2_2 from a charge with stearic acid, at IW-buffered fH_2, contains 72–85 rel.% H_2O, lower alkanes and slightly higher O-bearing HCs than reduced fluids (Fig. 7b). According to calculations by Litasov etal. (2014) based on equations of state for real gases from Zhang and Duan (2009), the H_2O molar fraction is as low as 0.2 in C-O-H fluids synthesized at 6.5 GPa, 1200 deg C, and fO_2 at IW but reaches 0.5 at fO_2

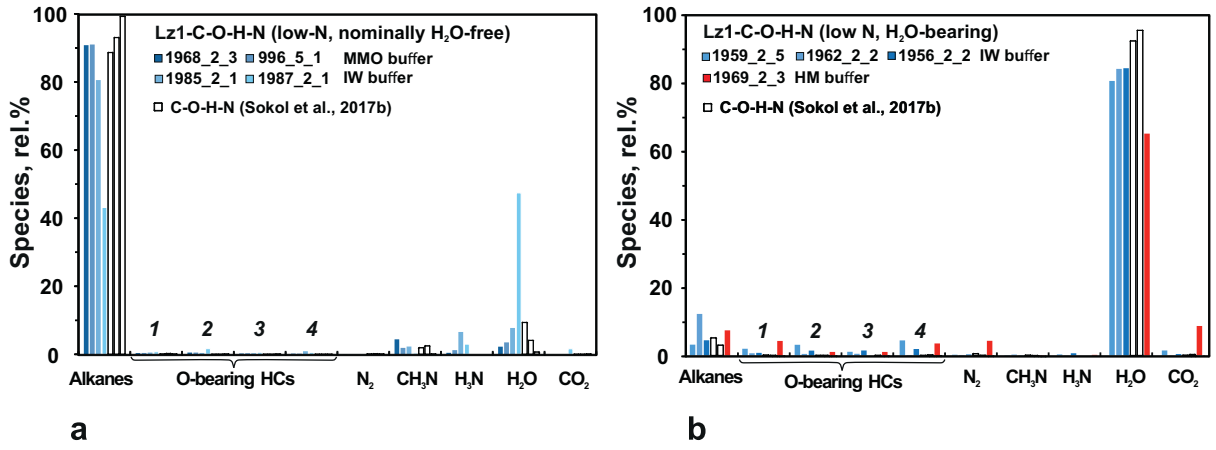

Fig. 7. Main species of N-poor fluid in the Lz1-C-O-H-N system at 5.5–7.8 GPa and 1150–1350°C. (a)Fluid composition obtained from nominally oxygen-free charges containing docosane (IW buffer) compared with species of a simplified C-O-H-N system (Sokol etal., 2017b); (b)Fluid composition obtained from oxygen-bearing charges containing stearic acid; *blue and red shaded zones* correspond, respectively, to IW and HM buffers. 1 = alcohols and ethers; 2 = aldehydes; 3 = ketones; 4 = carboxylic acids. *Grey bars* are species of a simplified C-O-H-N system.

buffered by the MMO equilibrium. Our results differ from those calculations because of fH_2 rather than fO_2 buffering. The oxygen fugacity in a sample ($fO_2{}^S$) with IW-bufferedfH_2 satisfies the equation of Boettcher etal. (1973):

$$fO_2^S = fO_2^B\left(\frac{fH_2O^S}{fH_2O^B}\right),$$

where fO_2^B is the buffer oxygen fugacity and fH_2O^S and fH_2O^B are, respectively, the sample and buffer water fugacities. It is clear from this equation that $fO_2^S < fO_2^B$ when C-H-O-N fluid in the inner capsule has a lower water fugacity than H-O fluid in the buffer assemblage. Oxygen fugacity will be the lowest in fluids synthesized from nominally oxygen-free charges at buffered fH_2 in the case of low fH_2O^S. According to our calculations (Sokol etal., 2017b), fO_2 in HCs-rich fluids obtained from such charges at 6.3 GPa and 1200–1400 deg C will be −2.5 Δlog fO_2 IW. However, fO_2^S may exceed fO_2^B in the case of an H_2O-rich fluid, because, at the P-T conditions of the experiments, fluid in the outer capsule was equilibrated with enstatite and coesite produced by talc decomposition, which, are more soluble in water-rich fluids (especially coesite) than lherzolitic minerals. In the case of $fO_2^S > fO_2^B$, H_2O contents in fluids will reach 85 rel.% and exceed the calculated values (Litasov etal., 2014). Generally, we estimate that the difference in relative activities of

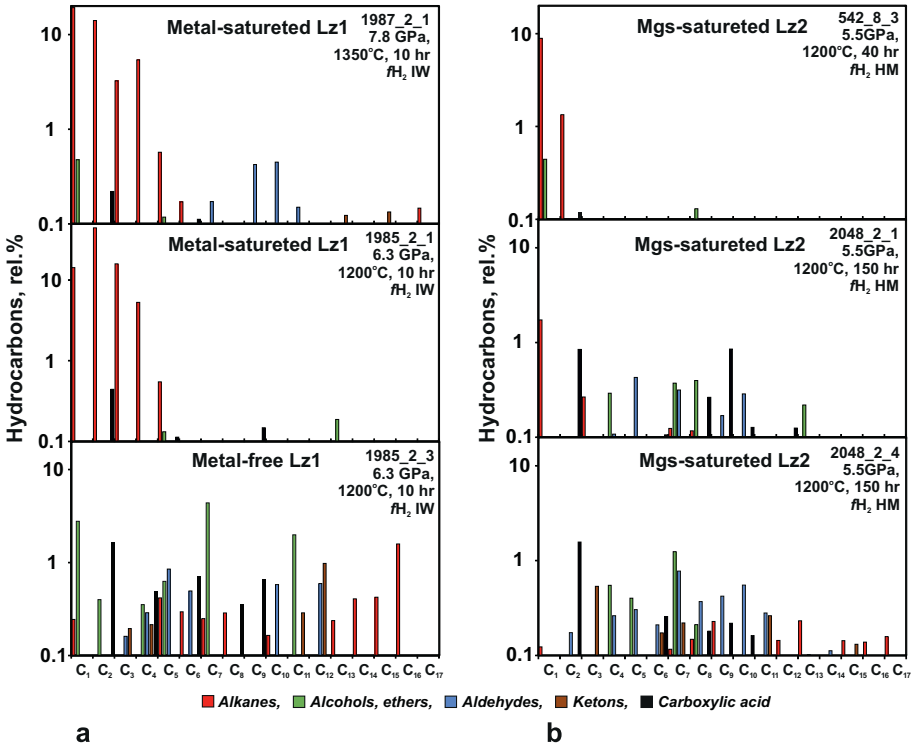

Fig. 8. Concentration of alkanes, alcohols and ethers, aldehydes, ketones and carboxylic acids with 1 to 17 carbon atoms in N-poor fluid after runs at 5.5–7.8 GPa and 1200–1350°C. (a)Lz1-C-O-H-N system (IW buffer); (b)Lz2-C-O-H-N system (HM buffer).

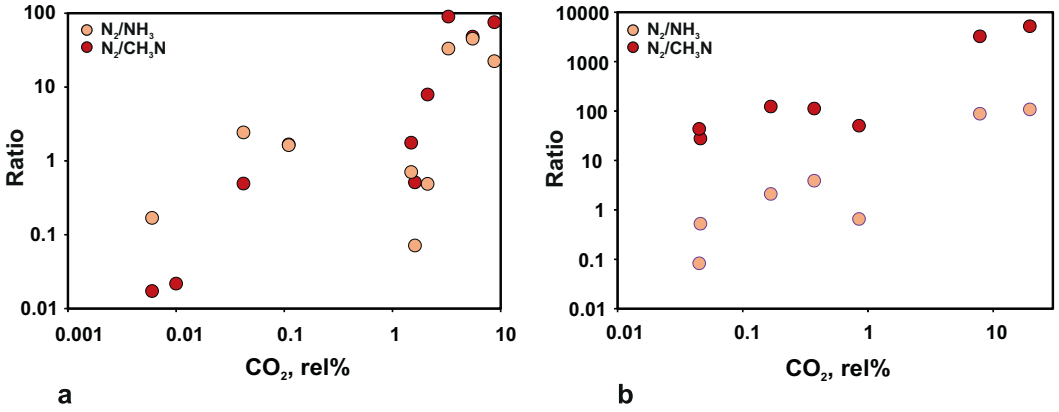

Fig. 9. Changes in N_2/NH_3 and N_2/CH_3N ratios in N-poor (a)and N-rich (b)fluids from the Lz1-C-O-H-N system with increasing CO_2.

water between the sample and the buffer provides variations of fO_2^S within ±2.5 Δlog fO_2IW at buffered fH_2 in the double-capsule technique.

Fluids synthesized from nominally nitrogen-free charges contain progressively smaller contents of lower alkanes as fO_2 increases, while H_2O and oxygenated HCs increase and heavy alkanes remain invariable (Figs. 7, 12). Fluids with CO_2 reaching 1–2 rel.%, which is typical of CW conditions (Foley, 2011), contain within 85 rel.% H_2O and at least 3–12 rel.% alkanes, as well as notable amounts of oxygenated HCs, especially alcohols and carboxylic acids. Fluids equilibrated with magnesite-saturated lherzolite at fO_2 about EMOD have at least 9 rel.% HCs (C_2-C_{13} species, Fig. 8b), with 1.7 to 10.5 rel.% alkanes, 1.3 to 10.8 rel.% O-bearing HCs, and relatively low H_2O (Fig. 12a, b).

Reduced N-poor fluids contain approximately equal amounts of NH_3 and CH_3N as main nitrogen species (Fig. 9a), but N_2 approaches the concentrations of NH_3 and CH_3N when fO_2 reaches CW and exceeds these concentrations upon further fO_2 increase to EMOD. In N-rich compositions, NH_3 and N_2 contents are similar even in ultra-reduced fluids equilibrated with Fe^0-bearing lherzolite (Fig. 9b). As fO_2 reaches the CW level, NH_3 becomes lower while most nitrogen exists as N_2, and the N_2/NH_3 ratio is within 100 at $CO_2 \geq 8$ rel.%. Note that CH_3N in N-rich fluids is a minor nitrogen host: its content does not exceed 1 rel.%, even in the ultra-reduced compositions.

The influence of silicate and metal phases on fluid composition is evident when our results are compared with those for the simplified C-O-H-N system at the same *P-T-fO*$_2$ values, with the same fH_2 buffering approach (Sokol etal., 2017a, 2017b) (Fig. 7): capsule material causes no marked influence on the contents of species in quenched fluids. The ultra-reduced fluids of these systems obtained at 5.5–7.8 GPa and 1150–1350 deg C, with <10 rel.% H_2O, are compositionally similar. They contain predominant light alkanes, with the CH_4/C_2H_6 ratio from 0.1 to 1.0. Therefore, the solid phases in lherzolite cause very little, if any, influence on HC speciation. At the same time, N-poor fluids in the lherzolite-C-O-H-N system contain as much CH_3N as those of the C-O-H-N system, but also commensurate amounts of NH_3 which is lacking in the simplified system. Moreover, the metal phase dissolves nitrogen (Table 4) which reduces its content in the fluid (Supplementary Fig. S4).

Light alkanes in H_2O-rich fluids are low in the simplified C-O-H-N and Lz-C-O-H-N systems (Fig. 7b), but fluids from both Lz1 and Lz2 contain notably greater concentrations of all oxygenated HCs, especially alcohols and carboxylic acids (Fig. 8). It can be noted that O-bearing HCs also reach relatively high concentrations in more oxidized fluids with fO_2 at EMOD. Their stability in such fluids may be due to partial dissolution of lherzolitic silicates in the fluid phase.

According to calculations by Sverjensky etal. (2014), large concentrations of dissolved carbon may be present as ionic organic species in upper mantle aqueous fluids. Particular eclogitic fluids at 5 GPa and 1140 deg C may contain dissolved organic carbon species such as aliphatic acid anions. Their stabilization is possible at strongly alkaline pH by dissolution of large amounts of Na^+ in fluids. At 1.0–2.1 GPa and 700–1200 deg C, the forsterite + enstatite assemblage is more soluble in H_2O-CO_2 fluids than in pure water, possibly, due to the formation of organic C–Mg–Si complexes (Tiraboschi etal., 2018). Thus, the formation of organic complexes in the fluids we synthesized can stabilize O-bearing HCs in the lherzolite-C-O-H-N system, unlike the simplified system C-O-H-N. Specifically, acetic acid reaching 1 rel.% in oxygenated fluids in runs #1985_2_3, 2048_2_1 and 2048_2_4 (Fig. 8) apparently occurs in the CH_3COO^- form at the *P-T* conditions of our experiments.

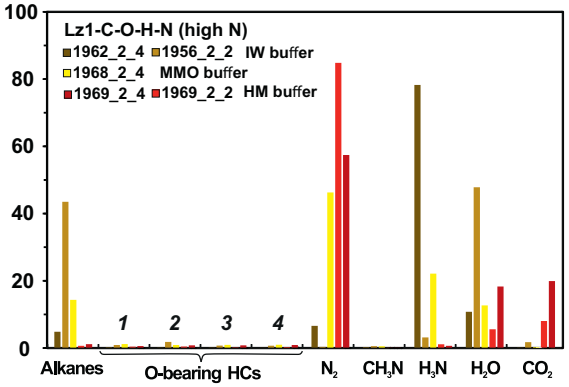

Fig. 10. Main species of N-rich fluid in the Lz1-C-O-H-N system. *Yellow shades* show runs with reduced IW and MMO external buffers; *red shades* correspond to runs with HM buffer. 1 = alcohols, ethers; 2 = aldehydes; 3 = ketones; 4 = carboxylic acids.

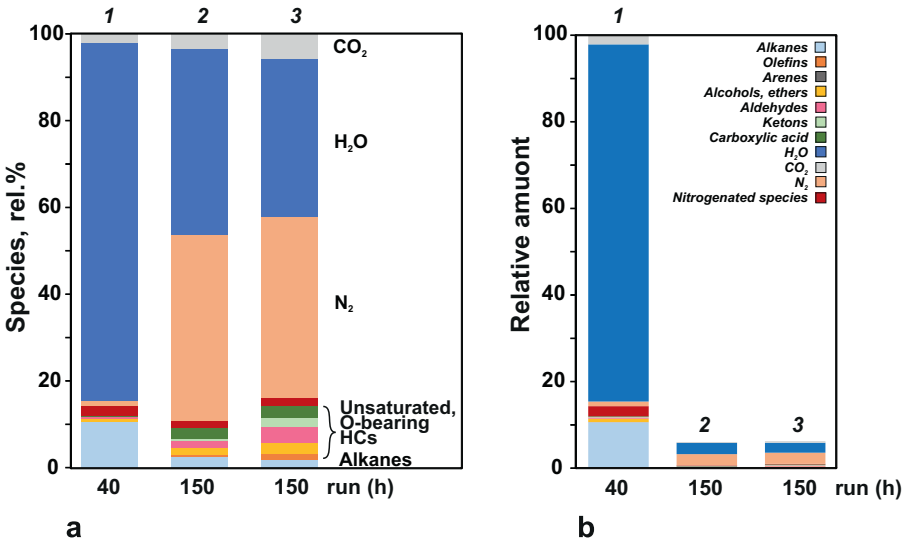

Fig. 11. Fluid composition changes upon carbonation of the Lz2-C-O-H-N system at 5.5 GPa and 1200°C as a result of hydrogen diffusion from capsule to HM buffer. 40-h run #542_8_3 (1); 150-h run #2048_2_1 (2); 150-h run #2048_2_4 (3).

The fluid composition in lherzolite changes notably at fO_2 of the EMOD equilibrium: CO_2 does not exceed 5 rel.%; total HCs (mainly C_2-C_{13} alkanes and oxygenated HCs) are never below 9 rel.% in fluids equilibrated with magnesite-bearing lherzolite at 5.5 GPa and 1200 deg C, even in 150-h runs. The formation of a Ca-Mg carbonate melt in the Lz2-C-O-H-N system at 5.5 GPa and 1200 deg C (run #2048_2_1) apparently leads to significant redistribution of volatiles between the melt and fluid phases. Proceeding from the high solubility of water in Ca-Na-Mg carbonate melts at 0.2 GPa reported by Keppler (2003), Ca-Mg carbonate melts can be expected to consume most H_2O, while the fluid becomes rich in N_2.

Generally, fluids equilibrated with Fe^0- and magnesite-saturated lherzolite samples (Lz1 and Lz2, respectively) differ markedly in HC speciation (Fig. 8): mostly C_1-C_4 alkanes in the former case but C_2-C_{13} alcohols and ethers, aldehydes, ketones, and carboxylic acids in the latter case. Water does not exceed 84 rel.% as fO_2 in the lherzolite-C-O-H-N systems increases and fluids evolve from HC-rich to CO_2-bearing compositions (Fig. 12a, b).

4.2. Metal phase composition

The metal phase in graphite-saturated samples of the Lz1-C-O-H-N system, in the presence of fluids with high HC and low nitrogen contents, has a ~10 wt.% deficit of totals and contains 5–6 wt.% Ni (Table 4). It does not melt under the applied *P-T* conditions, judging by the morphology of metal grains and the absence of quench textures, and hence can be either Fe_3C or Fe_7C_3. As shown by Sokol etal. (2017c), nitrogen is poorly soluble in Fe_3C and remains within 0.5 wt.% even in the case of equilibrium with an N-rich metal melt. This result is consistent with very low nitrogen contents (below EDS detection) in iron carbide equilibrated with fluid containing 2.6–4.6 rel.% nitrogen, mainly as NH_3 and CH_3N (Table 2). Since Ni-bearing carbides Fe_7C_3 (to molar X_{Ni} = Ni/(Fe + Ni) = 0.11) and Fe_3C (to X_{Ni} = 0.24) are stable at subsolidus in the Fe-Ni-C system at 10 GPa (Rohrbach etal., 2014), the presence of Fe_7C_3 appears more probable at <1300 deg C (Lord etal., 2009) while Fe_3C may be stable at 1300 and 1350 deg C (Sokol etal., 2017c).

The metal phase of N-rich samples in this study contains 3 to 8.5 wt.% N (Table 4), or 12 to 27 at.% (Fig. 5a), while the morphology and texture of grains indicates the absence of melting (Fig. 2c, d). With its high nitrogen contents, the phase can hardly be carbide but rather may be iron nitride (ε-Fe_3N), which is stable at high pressures and contains 6.0–7.3 wt.% N and up to 2.0–2.5 wt.% C in equilibrium with a C– and N-rich metal melt (Sokol etal., 2017c). Ni nitrides are stable up to ~1350 deg C at 1 bar, and the high-temperature ε-Ni_3N phase is isostructural with iron nitride (Guillermet and Frisk, 1991). Therefore, Ni-bearing iron nitride can be reasonably expected to be stable at high *P-T* conditions. Nitrogen decrease with Ni increase in the nitride phase (Fig. 5b) may indicate lower nitrogen solubility in Ni-rich iron nitride.

4.3. Phase relations in the lherzolite-C-O-H-N system

Analysis of phase relations should begin with an estimation whether the lherzolite-C-O-H-N system at experimental *P-*fO_2 parameters was above the second critical endpoint, when the solidus terminated and the silicate melt and the fluid became compositionally similar. This is potentially possible, because the solidus of the basalt–H_2O system terminates between 5 and 6 GPa (Kessel etal., 2005). As shown by Green etal. (2010), subsolidus water-rich fluid in equilibrium with lherzolite has a high solute content at 6 GPa, but hydrous silicate melt and water-rich fluid remain compositionally separated. Below the second critical endpoint, H_2O-rich fluids at 6.0 GPa and 1100 deg C may contain up to 15 wt.% dissolved silicate, or slightly more (Dvir and Kessel, 2017; Stalder etal., 2001). In the reduced CH_4-bearing fluid, the solubility of lherzolitic silicates was found to be limited or even negligible at 3–6 GPa (Sokol etal., 2010; Taylor and Green, 1988). The absence of quenched solutes from all fluids we obtained suggests that silicates are poorly soluble in fluids containing HCs and N-bearing species while the lherzolite-C-O-H-N system is below the second critical endpoint within the studied P-fO_2 range.

The results show that the fluid-lherzolite interaction, almost over the entire *P-T-*fO_2 range, does not cause lherzolite melting. In the lherzolite-C-O-H-N system, the first batches of carbonate melt (Fig. 6) appear at 5.5 GPa and 1200 deg C only when fO_2 reaches the EMOD equilibrium and lherzolite becomes carbonated at the account of HCs and C^0 oxidation. In the metal-saturated Lz1-C-O-H-N system at 5.5, 6.3 and 7.8 GPa and 1150 to 1350 deg C, olivine, orthopyroxene, clinopyroxene, garnet, and a metal phase (Ni-bearing iron carbide or nitride) coexists with fluid in some runs (Figs. 4, 7, 8, S2a). At higher fO_2, Ni in the metal phase can reach 25 wt.%. Oxygen fugacity near CW leads to oxidation of the metal phase and Mg# decrease in olivine and orthopyroxene (Fig. 4a). The range of Mg# suggests that FeO is mainly dissolved in olivine and orthopyroxene, while the Ol/Opx ratio is expected to increase. As the fluid fraction in the system increases to ≥0.2,

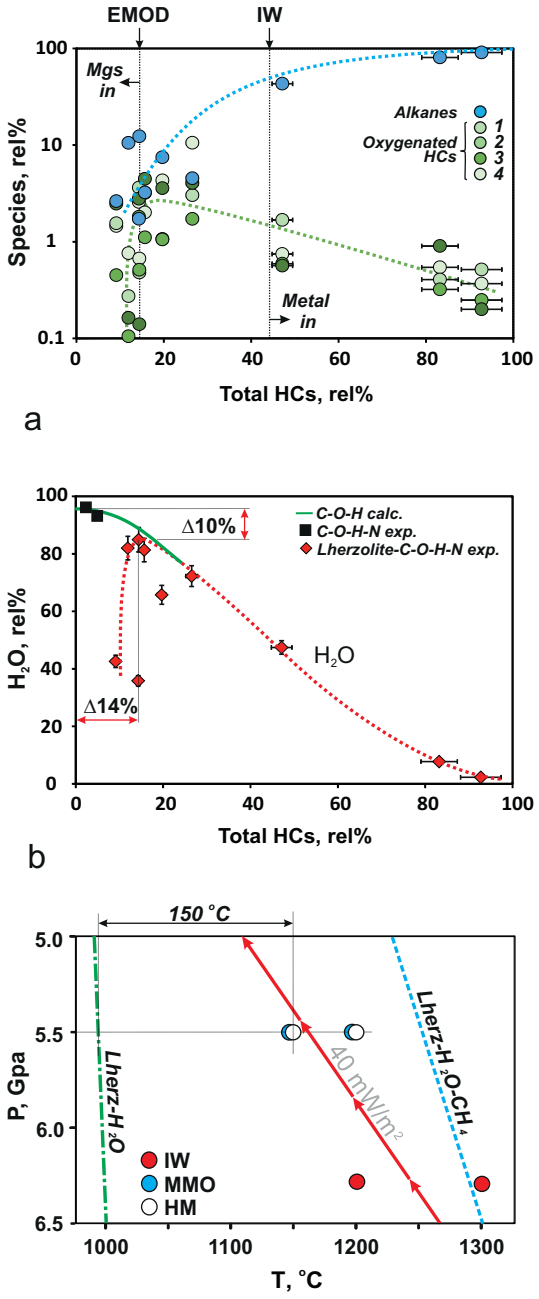

Fig. 12. Composition changes of N-poor fluid in the lherzolite-C-O-H-N system with fO_2 changes and effect of fluid composition on the system solidus. (a)Trends of alkanes and O-bearing HCs at increasing fO_2; (b)Trends of H_2O at increasing fO_2. Calculated H_2O contents in the C-O-H system near CW (Foley, 2011); experimental results for a simplified system C-O-H-N (Sokol etal., 2017b) are shown for comparison; (c)effect of fluid composition on lherzolite solidus. Lherz-H_2O is water-saturated lherzolite solidus (Green, 2015). The position of Lherz-H_2O-CH_4 solidus at water activity $aH_2O = 0.85$ according to Taylor and Green (1988). *Red arrows* show P-T trend with fluid ascent along the 40 mW/m^2 geotherm. 1 = alcohols and ethers; 2 = aldehydes; 3 = ketones; 4 = carboxylic acids.

Na leaches from clinopyroxene into the fluid (Supplementary Fig. S2b, c). This leads to disappearance of the jadeite component from clinopyroxene because Al_2O_3 in orthopyroxene is about the equilibrium content at the experimental *P-T* conditions (Table 3); clinopyroxene and garnet disappear when the fluid fraction reaches 0.35–0.4 (Table 2). Previously Kovács etal. (2012), Green etal. (2010, 2014) and Green (2015) showed that Na and K contents of clinopyroxene and pargasite systematically varied with the amount of water-rich fluid in the lherzolite-H_2O system at $P < 5.0$ GPa.

In the Lz2-C-O-H-N system, olivine, orthopyroxene, clinopyroxene, and garnet coexists with magnesite and the fluid phase at 5.5 GPa and 1200 deg C and fO_2 from slightly below CW to EMOD(Figs. 4b, S2a). Silicate compositions are almost identical to those in the starting xenolith, except for lower Ca# in clinopyroxene in a magnesite-free charge in an Au capsule (Figs. 4b, S2c). Carbonation of lherzolite by CO_2 from the fluid phase causes replacement of olivine and orthopyroxene by magnesite (with 1.8 wt.% CaO and 4 wt.% FeO) and clinopyroxene, respectively. The first batches of carbonate melt appear in carbonated lherzolite in the presence of a fluid phase, in a 150-h run (Fig. 6; Table 2).

Phase relations in the N-rich system Lherzolite-C-H-O-N at 5.5–7.8 GPa have been studied for the first time. In the case of a nominally N-free Lherzolite-C-H-O system investigated over a large range of pressures and low fO_2(Litasov etal., 2014; Taylor and Green, 1988), samples also contained more or less nitrogen from trapped air, as in our N-poor runs. In the cited works, fO_2 was buffered in a similar way to the one we used, with tungsten carbide/tungsten oxide (IW + 1 log unit) (Taylor and Green, 1988) or MMO (IW + 1 log unit) and IW(Litasov etal., 2014). Our data on the phase relations in the Lherzolite-C-H-O-N system for this fO_2 range agree well with the results of Taylor and Green (1988) and Litasov etal. (2014). Meanwhile, GC–MS analysis provided quantitative proof for the earlier inference that HCs can suppress the activity of water in fluids at $P > 5.0$ GPa. As a result, peridotite does not melt upon interaction with reduced fluids at typical upper mantle thermal conditions.

Previously, the solidi of water-saturated carbon-free lherzolite and the lherzolite-H_2O-CO_2 system, both nominally nitrogen-free, were studied with H_2O as a source of water and with carbonate, CO_2 or graphite/diamond as a source of carbon (Dvir and Kessel, 2017; Green, 2015; Green etal., 2010, 2014; Grove etal., 2006; Kovács etal., 2012; Wallace and Green, 1988). Hydrogen fugacity, without external buffering, was controlled by the furnace assembly near the Ni-NiO buffer (Boettcher etal., 1973), while the fluid lacked HCs. Unlike that case, water and carbon in our experiments came from stearic acid which oxidized in the samples at very low HM-buffered fH_2.

The water-saturated solidus of enriched lherzolite (with $H_2O >$ 4000 ppm) in the range of pressures we used is close to 1000 deg C (Green, 2015). In order to highlight the effect of HC impurity in the water-rich fluid phase on the lherzolite solidus near CW, we had to account for leaching of alkalis by the fluid, which leaves an increasingly refractory lherzolite (Green, 2015; Green etal., 2010, 2014; Kovács etal., 2012). The problem was solved with a test run at 5.5 GPa and 1200 deg C with a carbon-free Lz2-H_2O charge (run #2048_2_3, 2.5 wt.% H_2O) where we observed batches of hydrous silicate melt (Fig. 3a). The absence of melting signatures in the sample with stearic acid (run #542_8_3) indicates that the presence of HCs stable to oxidation in the lherzolite-C-O-H-N system does reduce water activity in the fluid phase at fO_2 between CW and EMOD. Comparison with data by Green (2015) shows that the lherzolite solidus in the presence of a H_2O-rich and HC-bearing fluid is 150 deg C above that in H_2O-saturated but carbon-free conditions (Fig. 1b). The difference is still greater with the data of Grove etal. (2006) extrapolated onto the region of pressures we used.

Conditions of formation of the first batches of carbonate melt entrapped as inclusions in olivine in run 2048_2_1 (5.5 GPa, 1200 deg C, and fO_2 at EMOD) agree with the available data. Namely, the lherzolite solidus varies from 900 to 1000 deg C at 4 GPa in the presence of 0.3 wt% H_2O and 0.5–2.5 wt% CO_2(Green, 2015; Wallace and Green, 1988), and is about 1050 deg C at 5–6 GPa, with 10 wt% H_2O and 5 wt% CO_2(Dvir and Kessel, 2017).

4.4. Fluid-rock interaction at the base of subcratonic lithosphere

The experimental data reveal the main features of fluid-rock interaction during ascent of volatiles from Fe^0-saturated asthenosphere into

relatively oxidized subcratonic lithosphere along the 40 mW/m^2 geotherm. Three main lherzolite mineral assemblages obtained experimentally at progressively increasing fO_2 coupled with decreasing P and T (namely, metal-bearing lherzolite → lherzolite → magnesite-bearing lherzolite) reproduce three main stages of interaction between percolating fluids and peridotitic mantle (Fig. 1a). The stability of the metal phase, magnesite (or carbonate melt), and the species containing HCs and N in the fluid during this interaction is expected to control the deep carbon and nitrogen cycles in the upper mantle.

Stage 1: Fluids enriched in light alkanes and depleted in both water and nitrogen (few wt.% NH_3 and CH_3N) interact with Fe^0-bearing peridotite, which leads to capture of some carbon by the metal phase and formation of Ni-bearing iron carbides Fe_3C and/or Fe_7C_3. Some carbon becomes immobilized by diamond crystallizing in the metal melt (Palyanov etal., 2012, 2013; Rohrbach etal., 2014; Smith etal., 2016). HC-bearing fluids with high nitrogen (24 to 78 rel.% NH_3 and 0.4 to 33 rel.% N_2) and low H_2O interacting with lherzolite cause nitrogen saturation of the metal phase and produce Ni-bearing iron nitride ε-Fe_3N (Fig. 5). Furthermore, high contents of NH_3 in the fluids facilitates nitrogen incorporation in silicates: 4 ppm in olivine, 210 ppm inorthopyroxene and clinopyroxene, and 60 ppm in garnet (Lietal.,2013). Fluids can selectively accumulate carbon while the metal phase can capture nitrogen (Sokol etal., 2018). As fO_2 increases and approaches the Fe-Ni alloy stability limit, nitrogen in nitride decreases to 3 wt.% while nickel increases to 25 wt.% (Fig. 5b).

Stage 2: Fluids interact with lherzolite free from metal at fO_2 between IW and CW(Fig. 1a), which is possible at depths shallower than 250 km (~7.8 GPa), outside the inferred domain of Fe-Ni alloy stability (Rohrbach and Schmidt, 2011). Carbon, being poorly soluble in silicates (Shcheka etal., 2006), can ascend with HCs among other fluid components, including Mg-, Si- and Na-bearing organic species (Sverjensky etal., 2014). Some NH_3 abundant in fluids percolating through lherzolite becomes immobilized by silicates. At the depths where fO_2 is near CW, water activity in H_2O-rich fluid is relatively low due to dilution with HCs (14 rel.% alkanes and oxygenated HCs) and N_2, which preclude the melting of lherzolite (Fig. 12a, b). Under these conditions, HC-bearing fluids store water and some carbon. Petrological data, along with the isotope fractionation factor of carbon ($\Delta C_{diamond\text{-}fluid}$), indicate that partial oxidation of methane-bearing fluids and release of C^0 can maintain the crystallization of diamond (Stachel and Luth, 2015; Thomassot etal., 2007). According to experimental evidence, the process of diamond formation in the fluid phase is possible only at high water contents and fO_2 near CW(Palyanov and Sokol, 2009; Sokol etal., 2009) and at low amounts of SiO_2 and MgO dissolved in the fluid phase (Sokol and Pal'yanov, 2008). Diamond formation is also favours nitrogen capture from fluids (Cartigny etal., 2001; Shireyetal., 2013). On the other hand, increasing N_2 in the fluid phase reduces the solubility of nitrogen in peridotite minerals to a few ppm (Li etal., 2013).

Stage 3: Water-rich fluids, containing up to 5 rel.% CO_2 and within 9 rel.% of alkanes, alkenes, and O-bearing HCs (Fig. 12a, b), react with lithospheric peridotite at fO_2 corresponding to the EMOD equilibrium, whereby carbonation of lherzolitic olivine and orthopyroxene produces clinopyroxene and magnesite, and the first batches of carbonate melt appear. Water-bearing carbonate melt, a good diamond growth medium, allows diamond crystallization (Palyanov and Sokol, 2009). Upon further oxidation, most of the carbon from fluids becomes immobilized in magnesite and/or carbonate melt. N_2, which is poorly soluble in carbonate melt, may reside in the fluid phase.

In general, our data show that asthenospheric HC fluids can be efficient carriers of carbon and water from Fe^0-saturated asthenosphere to subcratonic lithosphere. The reason is that the ascent and partial oxidation of fluids at a heat flux of 40 mW/m^2 may occur without hydrous redox melting of peridotite at fO_2 near CW(Fig. 12c), because water activity in the fluid becomes suppressed by HC species stable to oxidation. As the fluids ascend to lithospheric depths where fO_2 reaches EMOD, oxidation of HC species produces carbonate-silicate melts in peridotite, which can be involved in metasomatic reactions and the generation of kimberlite magma within subcratonic lithosphere.

5. Conclusions

Fluid-rock interactions simulated by experiments with the lherzolite-C-O-H-N system at 5.5–7.8 GPa, 1150–1350 deg C, and fO_2 from 2.5 log units below to 3.5 log units above IW, largely control the fluid composition and the mobility of volatiles in the asthenosphere and at the base of the subcratonic lithosphere. During their ascent through peridotitic mantle at progressively increasing fO_2 and decreasing T and P, fluids interact successively with three main types of lherzolite mineral assemblages: metal-bearing lherzolite → lherzolite → magnesite-bearing lherzolite. The interactions are realized through several processes: formation of stable HC and N-bearing species; dissolution of carbon and nitrogen in the metal phase and NH_3 in silicates; oxidation of HCs and crystallization of magnesite. Fluids rising from asthenospheric depths to the base of the subcratonic lithosphere change their compositions from abundant H_2O (up to 50 rel.%) and C_1-C_4 alkanes, minor amounts of alkenes and O-bearing HCs (carbon species), as well as NH_3 and CH_3N (main nitrogen species), to high H_2O (up to 85 rel.%) and lower contents of alkanes, O-bearing HCs, and N_2 (within 9–14 rel.%). The presence of N-bearing species and HCs stable to oxidation in the lherzolite-C-O-H-N system at the *P-T* conditions of the subcratonic lithospheric base, and at fO_2 near CW, can suppress water activity in fluids and increase the lherzolite solidus to at least 150 deg C above the water-saturated solidus. Water-rich fluids with 9–14 rel.% HCs in the lherzolite-C-O-H-N system are stable at fO_2 between CW and EMOD. Therefore, HC-bearing fluids can percolate into more oxidized mantle domains at a typical heat flux of 40 mW/m^2 without being involved in hydrous redox melting and generation of silicate melts. When reaching the subcratonic lithosphere with fO_2 at the EMOD equilibrium, fluids carrying residual HCs can cause carbonatite metasomatism of peridotite and contribute to the generation of carbonatite magma.

Supplementary data to this article can be found online at https://doi.org/10.1016/j.lithos.2018.08.025.

Acknowledgments

We wish to thank Yury Borzdov and Alexander Khokhryakov for their assistance throughout the study. We deeply appreciate the help Rodney Grapes in preparing the manuscript. The manuscript profited much from thoughtful reviews by David H. Green and an anonymous reviewer. The research was performed by a grant of the Russian Science Foundation(16-17-10041).

References

Boettcher, A.L., Mysen, B., Allen, J.C., 1973. Techniques for the control of water fugacity and oxygen fugacity for experimentation in solid-mediahigh-pressure apparatus. J. Geophys. Res. 78 (26), 5898–5901.
Cartigny, P., Harris, J.W., Javoy, M., 2001. Diamond genesis, mantle fractionations and mantle nitrogen content: A study of ^{13}C-N concentrations in diamonds. Earth Planet. Sci. Lett. 185 (1–2), 85–98.
Day, H.W., 2012. A revised diamond-graphite transition curve. Am. Mineral. 97 (1), 52–62.
Doucet, L.S., Ionov, D.A., Golovin, A.V., 2013. The origin of coarse garnet peridotites in cratonic lithosphere: new data on xenoliths from the Udachnaya kimberlite, central Siberia. Contrib. Mineral. Petrol. 165 (6), 1225–1242.
Dvir, O., Kessel, R., 2017. The effect of CO2 on the water-saturated solidus of K-poor peridotite between 4 and 6 GPa. Geochim. Cosmochim. Acta 206, 184–200.
Foley, S., 2011. A reappraisal of redox melting in the Earth's mantle as a function of tectonic setting and time. J. Petrol. 52, 1363–1391.
Foustoukos, D.I., Seyfried, W.E., 2004. Hydrocarbons in hydrothermal vent fluids: the role of chromium-bearing catalysts. Science 304, 1002–1005.
Goncharov, A.G., 2012. Thermal state, oxygen fugacity and C-O-H fluid speciation in cratonic lithospheric mantle: new data on peridotite xenoliths from the Udachnaya kimberlite. Siberia. Earth Planet. Sci. Lett. 357, 99–110.
Green, D.H., 2015. Experimental petrology of peridotites, including effects of water and carbon on melting in the Earth's upper mantle. Phys. Chem. Miner. 42 (2), 95–122.

Green, D.H., Hibberson, W.O., Kovács, I., Rosenthal, A., 2010. Water and its influence on the lithosphere–asthenosphere boundary. Nature 467 (7314), 448.
Green, D.H., Hibberson, W.O., Rosenthal, A., Kovács, I., Yaxley, G.M., Falloon, T.J., Brink, F., 2014. Experimental study of the influence of water on melting and phase assemblages in the upper mantle. J. Petrol. 55, 2067–2096.
Griffin, W.L., Huang, J.X., Thomassot, E., Gain, S.E., Toledo, V., O'Reilly, S.Y., 2018. Super-reducing conditions in ancient and modern volcanic systems: sources and behaviour of carbon-rich fluids in the lithospheric mantle. Mineral. Petrol.:1–14 https://doi.org/10.1007/s00710-018-0575-x.
Grove, T.L., Chatterjee, N., Parman, S.W., Medard, E., 2006. The influence of H_2O on mantle wedge melting. Earth Planet. Sci. Lett. 249, 74–89.
Guillermet, A.F., Frisk, K., 1991. Thermodynamic properties of Ni nitrides and phase stability in the Ni-N system. Int. J. Thermophys. 12, 417–431.
Hasterok, D., Chapman, D.S., 2011. Heat production and geotherms for the continental lithosphere. Earth Planet. Sci. Lett. 307, 59–70.
Horita, J., Berndt, M.E., 1999. Abiogenic methane formation and isotopic fractionation under hydrothermal conditions. Science 285, 1055–1057.
Huizenga, J.M., Crossingham, A., Viljoen, F., 2012. Diamond precipitation from ascending reduced fluids in the Kaapvaal lithosphere: thermodynamic constraints. Compt. Rendus Geosci. 344 (2), 67–76.
Jacob, D.E., Kronz, A., Viljoen, K.S., 2004. Cohenite, native iron and troilite inclusions in garnets from polycrystalline diamond aggregates. Contrib. Mineral. Petrol. 146, 566–576.
Kaminsky, F.V., Wirth, R., 2011. Iron carbide inclusions in lower-mantle diamond from Juina, Brazil. Canad. Mineral. 49, 555–572.
Kaminsky, F., Wirth, R., 2017. Nitrides and carbonitrides from the lowermost mantle and their importance in the search for Earth's "lost" nitrogen. Am. Mineral. 102 (8), 1667–1676.
Keppler, H., 2003. Water solubility in carbonatite melts. Am. Mineral. 88 (11−12), 1822–1824.
Kessel, R., Ulmer, P., Pettke, T., Schmidt, M.W., Thompson, A.B., 2005. The water–basalt system at 4 to 6 GPa: phase relations and second critical endpoint in a K-free eclogite at 700 to 1400 C. Earth Planet. Sci. Lett. 237 (3–4), 873–892.
Kolesnikov, A.Y., Saul, J.M., Kutcherov, V.G., 2017. Chemistry of hydrocarbons under extreme thermobaric conditions. ChemistrySelect 2, 1336–1352.
Kovács, I., Green, D.H., Rosenthal, A., Hermann, J., O'Neill, H.S.C., Hibberson, W.O., Udvardi, B., 2012. An experimental study of water in nominally anhydrous minerals in the upper mantle near the water-saturated solidus. J. Petrol. 53 (10), 2067–2093.
Li, Y., Keppler, H., 2014. Nitrogen speciation in mantle and crustal fluids. Geochim. Cosmochim. Acta 129, 13–32.
Li, Y., Wiedenbeck, M., Shcheka, S., Keppler, H., 2013. Nitrogen solubility in upper mantle minerals. Earth Planet. Sci. Lett. 377, 311–323.
Litasov, K.D., Shatskiy, A., Ohtani, E., 2014. Melting and subsolidus phase relations in peridotite and eclogite systems with reduced C-O-H fluid at 3–16 GPa. Earth Planet. Sci. Lett. 391, 87–99.
Lobanov, S.S., Chen, P.N., Chen, X.J., Zha, C.S., Litasov, K.D., Mao, H.K., Goncharov, A.F., 2013. Carbon precipitation from heavy hydrocarbon fluid in deep planetary interiors. Nat. Commun. 4.
Lord, O.T., Walter, M.J., Dasgupta, R., Walker, D., Clark, S.M., 2009. Melting in the Fe-C system to 70 GPa. Earth Planet. Sci. Lett. 284, 157–167.
Luth, R.W., 2014. Volatiles in Earth's mantle. Treatise on Geochemistry 3.9. Elsevier, Oxford, pp. 355–391.
Matveev, S., Ballhaus, C., Fricke, K., Truckenbrodt, J., Ziegenben, D., 1997. Volatiles in the Earth's mantle: I. Synthesis of CHO fluids at 1273 K and 2.4 GPa. Geochim. Cosmochim. Acta 61 (15), 3081–3088.
Mikhail, S., Sverjensky, D.A., 2014. Nitrogen speciation in upper mantle fluids and the origin of Earth's nitrogen-rich atmosphere. Nat. Geosci. 7, 816–819.
Palyanov, Y.N., Sokol, A.G., 2009. The effect of composition of mantle fluids/melts on diamond formation processes. Lithos 112, 690–700.
Palyanov, Yu.N., Borzdov, Yu.M., Khokhryakov, A.F., Kupriyanov, I.N., Sokol, A.G., 2010. Effect of nitrogen impurity on diamond crystal growth processes. Cryst. Growth Des. 10, 3169–3175.
Palyanov, Y.N., Borzdov, Y.M., Kupriyanov, I.N., Khokhryakov, A.F., 2012. Effect of H_2O on diamond crystal growth in metal–carbon systems. Cryst. Growth Des. 12 (11), 5571–5578.
Palyanov, Yu.N., Bataleva, Y.V., Sokol, A.G., Borzdov, Y.M., Kupriyanov, I.N., Reutsky, V.N., Sobolev, N.V., 2013. Mantle–slab interaction and redox mechanism of diamond formation. Proc. Natl. Acad. Sci. U. S. A. 110, 20408–20413.
Rohrbach, A., Schmidt, M.W., 2011. Redox freezing and melting in the Earth's deep mantle resulting from carbon-iron redox coupling. Nature 472, 209.
Rohrbach, A., Ghosh, S., Schmidt, M.W., Wijbrans, C.H., Klemme, S., 2014. The stability of Fe–Ni carbides in the Earth's mantle: evidence for a low Fe–Ni–C melt fraction in the deep mantle. Earth Planet. Sci. Lett. 388, 211–221.
Shcheka, S.S., Wiedenbeck, M., Frost, D.J., Keppler, H., 2006. Carbon solubility in mantle minerals. Earth Planet. Sci. Lett. 245 (3–4), 730–742.
Shirey, S.B., Cartigny, P., Frost, D.J., Keshav, S., Nestola, F., Nimis, P., Walter, M.J., 2013. Diamonds and the geology of mantle carbon. Rev. Mineral. Geochem. 75, 355–421.
Smith, E.M., Shirey, S.B., Nestola, F., Bullock, E.S., Wang, J., Richardson, S.H., Wang, W., 2016. Large gem diamonds from metallic liquid in Earth's deep mantle. Science 354, 1403–1405.
Sobolev, N.V., Lavrentev, Yu.G., Pospelova, L.N., Sobolev, E.V., 1969. Chrome pyropes from Yakutian diamonds. Dokl. Akad. Nauk SSSR 189, 162–165 (in Russian).
Sobolev, N.V., Efimova, E.S., Pospelova, L.N., 1981. Native iron in Yakutian diamonds and its mineral assemblage. Sov. Geol. Geophys. 22, 25–28.
Sokol, A.G., Pal'yanov, Y.N., 2008. Diamond formation in the system $MgO–SiO_2–H_2O–C$ at 7.5 GPa and 1600 deg C. Contrib. Mineral. Petrol. 155 (1), 33–43.
Sokol, A.G., Palyanova, G.A., Palyanov, Yu.N., Tomilenko, A.A., Melenevsky, V.N., 2009. Fluid regime and diamond formation in the reduced mantle: experimental constraints. Geochim. Cosmochim. Acta 73, 5820–5834.
Sokol, A.G., Palyanov, Y.N., Kupriyanov, I.N., Litasov, K.D., Polovinka, M.P., 2010. Effect of oxygen fugacity on the H_2O storage capacity of forsterite in the carbon-saturated systems. Geochim. Cosmochim. Acta 74 (16), 4793–4806.
Sokol, A.G., Borzdov, Yu.M., Palyanov, Yu.N., Khokhryakov, A.F., 2015a. High-temperature calibration of a multi-anvilhigh-pressure apparatus. High Pressure Res. 35, 139–147.
Sokol, A.G., Khokhryakov, A.F., Palyanov, Y.N., 2015b. Composition of primary kimberlite magma: constraints from melting and diamond dissolution experiments. Contrib. Mineral. Petrol. 170 (3), 26.
Sokol, A.G., Palyanov, Y.N., Tomilenko, A.A., Bul'bak, T.A., Palyanova, G.A., 2017a. Carbon and nitrogen speciation in nitrogen-richC–O–H–N fluids at 5.5–7.8 GPa. Earth Planet. Sci. Lett. 460, 234–243.
Sokol, A.G., Tomilenko, A.A., Bul'bak, T.A., Palyanova, G.A., Sokol, I.A., Palyanov, Y.N. 2017b. Carbon and Nitrogen Speciation in N-poorC-O-H-N Fluids at 6.3 GPa and 1100–1400 deg C. Sci. Rep.7, 706. DOI:https://doi.org/10.1038/s41598-017-00679-7.
Sokol, A.G., Kruk, A.N., Seryotkin, Y.V., Korablin, A.A., Palyanov, Y.N., 2017c. Phase relations in the $Fe–Fe_3C–Fe_3N$ system at 7.8 GPa and 1350 deg C: Implications for carbon and nitrogen hosts in Fe^0-saturated upper mantle. Phys. Earth Planet. Inter. 265, 43–53.
Sokol, A.G., Tomilenko, A.A., Bul'bak, T.A., Kruk, A.N., Zaikin, P.A., Sokol, I.A., Palyanov, Y.N., 2018. The Fe–C–O–H–N system at 6.3–7.8 GPa and 1200–1400 deg C: implications for deep carbon and nitrogen cycles. Contrib. Mineral. Petrol. 173 (6), 47.
Stachel, T., Luth, R.W., 2015. Diamond formation—where, when and how? Lithos 220, 200–220.
Stachel, T., Harris, J.W., Brey, G.P., 1998. Rare and unusual mineral inclusions in diamonds from Mwadui, Tanzania. Contrib. Mineral. Petrol. 132, 34–47.
Stagno, V., Ojwang, D.O., McCammon, C.A., Frost, D.J., 2013. The oxidation state of the mantle and the extraction of carbon from Earth's interior. Nature 493, 84.
Stalder, R., Ulmer, P., Thompson, A., Günther, D., 2001. High pressure fluids in the system $MgO–SiO_2–H_2O$ under upper mantle conditions. Contrib. Mineral. Petrol. 140 (5), 607–618.
Sverjensky, D.A., Stagno, V., Huang, F., 2014. Important role for organic carbon in subduction-zone fluids in the deep carbon cycle. Nat. Geosci. 7, 909.
Taylor, W.R., Green, D.H., 1988. Measurement of reduced peridotite-COH solidus and implications for redox melting of the mantle. Nature 332, 349–352.
Thomassot, E., Cartigny, P., Harris, J.W., Viljoen (Fanus), K.S., 2007. Methane-related diamond crystallization in the Earth's mantle: stable isotope evidences from a single diamond-bearing xenolith. Earth Planet. Sci. Lett. 257, 362–371.
Tiraboschi, C., Tumiati, S., Sverjensky, D., Pettke, T., Ulmer, P., Poli, S., 2018. Experimental determination of magnesia and silica solubilities in graphite-saturated and redox-bufferedhigh-pressureCOH fluids in equilibrium with forsterite+ enstatite and magnesite+ enstatite. Contrib. Mineral. Petrol. 173 (1), 2.
Wallace, M.E., Green, D.H., 1988. An experimental determination of primary carbonatite magma composition. Nature 335 (6188), 343.
Yang, X., Keppler, H., Li, Y., 2016. Molecular hydrogen in mantle minerals. Geochem. Perspect Lett. 2, 160–168.
Yaxley, G.M., Berry, A.J., Kamenetsky, V.S., Woodland, A.B., 2012. An oxygen fugacity profile through the Siberian Craton— Fe K-edgeXANES determinations of Fe3+/ΣFe in garnets in peridotite xenoliths from the Udachnaya East kimberlite. Lithos 140, 142–151.
Zhang, C., Duan, Z., 2009. A model for C–O–H fluid in the Earth's mantle. Geochim. Cosmochim. Acta 73 (7), 2089–2102.